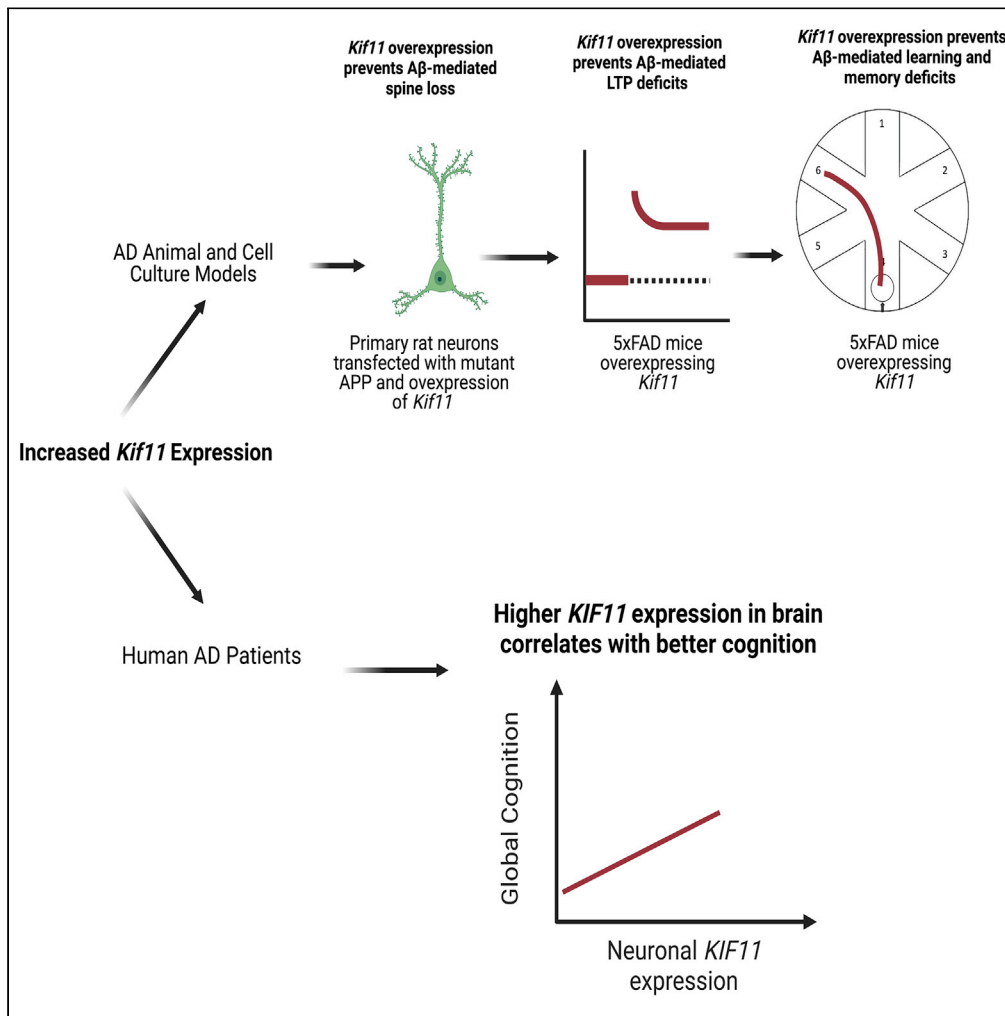


Article

Increased *KIF11*/kinesin-5 expression offsets Alzheimer A β -mediated toxicity and cognitive dysfunction



Esteban M. Lucero, Ronald K. Freund, Alexandra Smith, ..., Mark L. Dell'Acqua, Heidi J. Chial, Huntington Potter

huntington.potter@cuanschutz.edu

Highlights

Cognitive deficits in 5xFAD mice are prevented by *Kif11* overexpression

Kif11 overexpression prevents deficits in long-term potentiation in 5xFAD mice

A β -mediated dendritic spine loss is blocked by *Kif11* overexpression

Higher *KIF11* expression in brain correlates with better cognition in AD patients



Article

Increased *KIF11/kinesin-5* expression offsets Alzheimer A β -mediated toxicity and cognitive dysfunction

Esteban M. Lucero,^{1,2,3,4} Ronald K. Freund,^{2,5} Alexandra Smith,^{6,7} Noah R. Johnson,^{1,2,3} Breanna Dooling,^{1,2,3,4} Emily Sullivan,⁵ Olga Prikhodko,⁵ Md. Mahiuddin Ahmed,^{1,2,3} David A. Bennett,^{8,9} Timothy J. Hohman,^{6,7} Mark L. Dell'Acqua,^{2,3,5} Heidi J. Chial,^{1,2,3,10} and Huntington Potter^{1,2,3,10,11,*}

SUMMARY

Previously, we found that amyloid-beta (A β) competitively inhibits the kinesin motor protein KIF11 (Kinesin-5/Eg5), leading to defects in the microtubule network and in neurotransmitter and neurotrophin receptor localization and function. These biochemical and cell biological mechanisms for A β -induced neuronal dysfunction may underlie learning and memory defects in Alzheimer's disease (AD). Here, we show that KIF11 overexpression rescues A β -mediated decreases in dendritic spine density in cultured neurons and in long-term potentiation in hippocampal slices. Furthermore, *Kif11* overexpression from a transgene prevented spatial learning deficits in the 5xFAD mouse model of AD. Finally, increased *KIF11* expression in neuritic plaque-positive AD patients' brains was associated with better cognitive performance and higher expression of synaptic protein mRNAs. Taken together, these mechanistic biochemical, cell biological, electrophysiological, animal model, and human data identify KIF11 as a key target of A β -mediated toxicity in AD, which damages synaptic structures and functions critical for learning and memory in AD.

INTRODUCTION

The Alzheimer's disease (AD) brain exhibits the characteristic pathology of amyloid deposits, comprised primarily of the amyloid- β (A β) peptide, and intracellular neurofibrillary tangles, comprised primarily of hyperphosphorylated forms of the microtubule associated protein tau. These hallmark pathological features of AD, in tandem with many reports elucidating the toxic effects of the A β peptide, led to the amyloid cascade hypothesis (Hardy and Higgins, 1992). This hypothesis postulates that the neuronal accumulation of the A β peptide, a cleavage product of the amyloid precursor protein (APP), initiates a cascade of molecular events that lead to the development and progression of the neuronal damage and cognitive deficits associated with AD. The toxic effects of A β induce microtubule instability that can be directly linked to cellular dysfunctions affecting synaptic plasticity, such as impaired organelle and receptor transport, decreased dendritic spine density, and altered cell cycle regulation that leads to chromosome mis-segregation (Ari et al., 2014; Geller and Potter, 1999; Golovyashkina et al., 2015; Potter et al., 2019; Spires et al., 2005; Umeda et al., 2015; Wei et al., 2010; Wu et al., 2010). (Roussarie et al., 2020). Additional studies showed that treatment with microtubule-stabilizing drugs can ameliorate some AD phenotypes, including cognitive deficits, in model systems (Fernandez-Valenzuela et al., 2020; Penazzi et al., 2016; Zhang et al., 2018). Taken together, these findings demonstrate that the microtubule network plays a major role in establishing and maintaining neuronal structures and functions that are necessary for learning and memory and are disrupted in neurodegenerative diseases, such as AD (Dent, 2017).

In our previous search for potential mechanisms by which A β causes neurotoxicity, we discovered that the microtubule motor proteins KIF11 (Kinesin-5/Eg5), KIF4A, and MCAK/KIF2C are inhibited by soluble A β oligomers in a dose-dependent manner (Borysov et al., 2011). The inhibition of this select set of motor proteins by A β leads to both microtubule and mitotic defects (Borysov et al., 2011). Furthermore, specific inhibition of KIF11 by the small molecule monastrol mimicked the toxic effects of A β on the microtubule network and on the localization and function of the p75 neurotrophin receptor and of the NMDA receptor

¹Department of Neurology, University of Colorado Anschutz Medical Campus, Aurora, CO, USA

²University of Colorado Alzheimer's and Cognition Center, University of Colorado Anschutz Medical Campus, Aurora, CO, USA

³Linda Crnic Institute for Down Syndrome, University of Colorado Anschutz Medical Campus, Aurora, CO, USA

⁴University of Colorado Program for Human Medical Genetics and Genomics, University of Colorado Anschutz Medical Campus, Aurora, CO, USA

⁵Department of Pharmacology, University of Colorado Anschutz Medical Campus, Aurora, CO, USA

⁶Vanderbilt Memory and Alzheimer's Center, Vanderbilt University Medical Center, Nashville, TN, USA

⁷Vanderbilt Genetics Institute, Vanderbilt University Medical Center, Nashville, TN, USA

⁸Rush Alzheimer's Disease Center, Rush University Medical Center, Chicago, IL, USA

⁹Department of Neurological Sciences, Rush University Medical Center, Chicago, IL, USA

¹⁰These authors contributed equally

¹¹Lead contact

*Correspondence: huntington.potter@cuanschutz.edu

<https://doi.org/10.1016/j.isci.2022.105288>



2B (NMDAR2B) neurotransmitter receptor. Michaelis–Menten kinetic analyses of KIF11 motor function showed that the inhibition by A β was competitive (Borysov et al., 2011). KIF11 is linked specifically to AD by the previously-reported association between a single nucleotide polymorphism (SNP) within the KIF11 haploblock region and both AD and type II diabetes, which is a major risk factor for AD (Feuk et al., 2005), as well as the finding that *KIF11* is expressed in post-mitotic neurons where it contributes to neuronal structure and function (Freixo et al., 2018; Freund et al., 2016; Kahn et al., 2015b). We also found that inhibition of rodent *Kif11* by A β leads to decreases in the cell surface abundance and functions of the p75 and NMDAR2B receptors and to deficits in hippocampal long-term potentiation (LTP) (Ari et al., 2014; Freund et al., 2016). These findings highlight the importance of KIF11 for key neuronal functions in *in vitro* and *ex vivo* model systems, suggest that A β -mediated inhibition of KIF11 in humans may contribute at least in part to the cognitive dysfunction observed in AD, and indicate that overriding A β -mediated inhibition of KIF11 might prevent deficits in learning and memory in AD patients. However, the *in vivo* role of KIF11 in learning and memory during normal aging and in AD remained to be elucidated.

KIF11, the only member of the kinesin-5 family found in vertebrates, is a plus end-directed microtubule motor protein in mammalian cells that is best known for its role in mitosis where it contributes to bipolar spindle formation and provides the force required to separate the centrosomes and attached sister chromatids during cell division (Blangy et al., 1995; Bodrug et al., 2020; Ferenz et al., 2010; Kapitein et al., 2005; Mann and Wadsworth, 2019). In addition to its role in cell division, KIF11 is required for protein synthesis and serves as a link between ribosomes and microtubules during interphase in mammalian cells (Bartoli et al., 2011). KIF11 has also been shown to bind to the plus ends of microtubules and to enhance polymerization *in vitro* by stabilizing tubulin at the growing end of the microtubules, providing evidence that KIF11 regulates microtubule dynamics (Chen and Hancock, 2015).

An early study identified mouse *Kif11* expression in post-mitotic neurons (Ferhat et al., 1998), and later studies showed that *Kif11* regulates axonal growth and contributes to dendritic architecture and spine formation, where inhibition, knockdown, or overexpression of *Kif11* led to abnormal neurite outgrowth (Freixo et al., 2018; Kahn et al., 2015b; Myers and Baas, 2007; Nadar et al., 2008). In addition to its role in regulating neuronal morphology, the functional impact of *Kif11* on neuronal microtubule dynamics and on interactions between microtubules has been shown to play a key role in regulating neuronal migration and growth cone dynamics (Falnikar et al., 2011; Nadar et al., 2008). Although previous studies evaluating the functions and expression of *KIF11* have focused primarily on mitotic cells, developing neurons, and migrating neuronal cells, its expression continues in mature adult neurons although at a markedly lower level than in developing neurons (Lin et al., 2011). Further, the Human Protein Atlas (<https://www.proteinatlas.org>) (Uhlen et al., 2015) describes continued KIF11 expression in the adult brain, primarily in neurons of the cerebral cortex, thus suggesting a continued function of *KIF11* in postmitotic neurons. One possible responsibility of *KIF11* in mature neurons is to promote dendritic spine morphogenesis and density during dendritic maturation (Freixo et al., 2018). In sum, KIF11 carries out key roles in neurons that derive from its microtubule interactions and contribute to neuronal cell morphology, development, migration, and function. These data highlight the importance of regulating *KIF11* expression and function not only for development, but also for the maintenance of neuronal structures important for learning and memory beyond neuronal maturation.

Taken together, the known cytoskeletal functions of KIF11 and our discovery that A β -mediated inhibition of KIF11 enzymatic activity is a key mechanism underlying A β toxicity unequivocally identify KIF11 as an essential target of A β in human AD. Therefore, we investigated whether the reversal of A β -mediated inhibition of KIF11 prevents AD phenotypes in several experimental systems and, most importantly, in human AD patients. Here, we report that A β -mediated inhibition of KIF11 that disrupts learning and memory may be prevented by increasing the expression of *KIF11* to preserve its key cellular functions. Specifically, we predicted that increased expression of *KIF11* would override its inhibition by A β and prevent or reduce cognitive deficits attributed to A β toxicity *in vivo* via the maintenance of dendritic spine density and hippocampal LTP. To test our hypothesis, we first determined whether KIF11 overexpression blocked A β -mediated decreases in dendritic spine density, a phenotype heavily associated with cognitive loss in AD (DeKosky and Scheff, 1990; Freund et al., 2016; Scheff et al., 2006; Terry et al., 1991). We also employed a primary neuron model of AD and transient transfection to determine how overexpressing wild-type *Kif11* (Myers and Baas, 2007) and/or a familial AD (FAD) mutant form of APP (APP_{Swe/Ind}) (Young-Pearse et al., 2007) affects neuronal structure and function. We then generated a new mouse model derived by

inating the 5xFAD Alzheimer's mouse model (Oakley et al., 2006) to a mouse that overexpresses mouse *Kif11* (Castillo et al., 2007) to yield *Kif11*-overexpressing 5xFAD mice (5xFAD-*Kif11*OE) and carried out electrophysiological, behavioral, and pathological studies to determine the effect(s) of increasing *Kif11* expression on A β -associated AD phenotypes. The AD mouse model studies allowed us to investigate whether overexpression of KIF11 can rescue deficits in LTP and dendritic spine density and improve learning and memory *in vivo*.

We also set out to translate the mouse and cell culture work to humans, by querying RNAseq data from the Religious Orders Study and the Rush Memory and Aging Project (ROS/MAP) (Bennett et al., 2018) to elucidate whether naturally occurring variation in *KIF11* mRNA expression levels correlates with cognitive performance in a cohort of older adults with or without amyloid pathology. Our results from analyzing the human data indicate that higher endogenous levels of KIF11 correlate with better cognitive performance in neuritic plaque-positive participants from the ROS/MAP study, which is in agreement with our results showing that enhanced expression of *Kif11* obviates multiple deleterious effects of the A β peptide observed in 5xFAD mice and in primary rat neurons. Our use of human derived data along with a multi-model investigation provides a mechanistic demonstration that KIF11 is a key and modifiable target of A β toxicity and suggests that increased *KIF11* expression may prevent deficits in learning and memory in AD.

RESULTS

Kif11 overexpression prevents A β -mediated loss of spine density in primary rat neurons

A β toxicity has been attributed to synaptic loss in AD patients as well as in cell and mouse models of AD (Freund et al., 2016; Hsieh et al., 2006; Ingelsson et al., 2004; Spires et al., 2005), DeKosky and Scheff (1990), Scheff et al. (2006). Considering the role of *Kif11* in maintaining neuronal morphology and structure, and in view of our previous finding that A β -mediated inhibition of KIF11 is one mechanism likely to contribute to dendritic spine loss in AD (Freund et al., 2016), we sought to determine whether overexpression of *Kif11* can block A β -mediated spine loss. To this end, we employed a cell culture model and overexpressed wild-type *Kif11* using transient transfection to determine whether acute *Kif11* overexpression alone impacts spine density. Transient transfection and overexpression of *Kif11* in rat primary neurons led to a dose-dependent decrease in spine density with increasing concentrations of added *Kif11*-expressing plasmid (Figure S1). When combined with our previous findings showing that treatment with the highly specific *Kif11* inhibitor monastrol also reduces dendritic spine density, these findings for *Kif11* overexpression indicate that *Kif11* activity likely has to be maintained in a narrow range to support its normal cellular functions. These findings also clearly illustrate the structural role of *Kif11* in dendrites and in dendritic spines and are in agreement with previous studies showing that *Kif11* regulates neuronal architecture (Freixo et al., 2018; Kahn et al., 2015a, 2015b; Yoon et al., 2005). In parallel, we also employed an AD-*Kif11*OE cell culture model system in which primary rat neurons were transiently transfected to express human APP harboring both the Swedish (K595N and M596L) and Indiana (V642F) mutations (APP_{Swe/Ind}) (Young-Pearse et al., 2007), which results in A β overproduction and familial AD/early-onset AD (FAD/EOAD) in humans (Mullan et al., 1992), with or without *Kif11* overexpression. We hypothesized that the detrimental effects of A β on dendritic spines, which are important for learning and memory (Spires et al., 2005; Wei et al., 2010), would be reduced by acute *Kif11* overexpression. In agreement with previously published reports, we found that transfection of APP_{Swe/Ind} alone led to significant spine loss, which can be attributed to A β production and toxicity. In contrast, co-transfection of the APP_{Swe/Ind} vector together with a low amount of the *Kif11* overexpression vector, which produced only a small amount of spine loss compared to control on its own (Figure S1), prevented dendritic spine loss from reaching the higher levels normally seen for APP_{Swe/Ind} transfection alone (Figures 1A and 1B). These data showing reduced APP_{Swe/Ind}-mediated spine loss in the presence of *Kif11* overexpression support our hypothesis that A β -mediated spine loss is due in part to inhibition of *Kif11* by A β (Freund et al., 2016).

As discussed later, we included analyses of human data provided by the ROS/MAP study to investigate the effects of *KIF11* expression on AD phenotypes. One analysis that we performed of the ROS/MAP dataset evaluated mRNA expression levels of *KIF11* and of genes that encode synaptic proteins (i.e., *SYNAPTOPHYSIN*, *VAMP1/2*, *SNAP25*, *COMPLEXIN-1/2*, *SYNTAXIN 1A*) (Figures S2A–S2C). In that analysis, we detected *KIF11* expression in the dorsolateral prefrontal cortex (DLPFC) in amyloid positive ROS/MAP participants, and identified the following trends: (1) increases in amyloid burden correlated with decreases in the mean mRNA expression of synaptic proteins, (2) increases in global cognition positively correlated with higher mean synaptic marker mRNA expression, and (3) greater *KIF11* expression

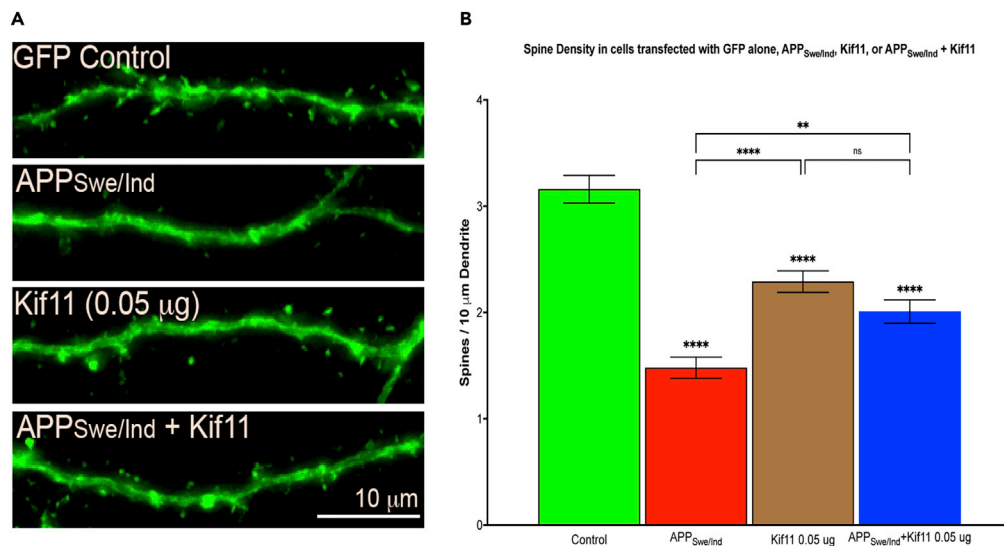


Figure 1. Moderate overexpression of Kif11 results in some dendritic spine loss but prevents more substantial spine loss mediated by A β in primary rat neurons

(A) Representative images of primary rat neurons transfected with a plasmid to express GFP alone (Control, N = 28), with a plasmid to express GFP together with a plasmid to express the human APP gene harboring both the Swedish double mutation (K595N and M596L) and the Indiana mutation (V642F) (APP_{Swe/Ind}, N = 30), with 0.05 μ g of a plasmid to express Kif11 (Kif11 0.05 μ g, N = 30), or with a plasmid to express APP_{Swe/Ind} together with a plasmid to express Kif11 (APP_{Swe/Ind} + Kif11 0.05 μ g, N = 28).

(B) Spine density measurements from primary rat neurons transfected with GFP alone (Control), with GFP and APP_{Swe/Ind} (APP_{Swe/Ind}), with GFP and Kif11 (Kif11 0.05 μ g), or with GFP, APP_{Swe/Ind}, and Kif11 (APP_{Swe/Ind} + Kif11 0.05 μ g). Statistical significance measured by ordinary one-way ANOVA with post-hoc Sidák's multiple comparisons test. Asterisks above each bar indicate statistical significance compared to control. **p < 0.01, ****p < 0.0001. Data represent mean with error bars representing the SEM.

positively associated with greater expression of synaptic marker mRNA in amyloid positive individuals (Figures S2A–S2C). These associations support our findings in primary rat neurons where overexpression of Kif11 blocked amyloid-mediated decreases in dendritic spine density. Thus, based on these data, we conclude that overexpression of Kif11 compensates for the damaging effects of A β on neuronal structures and functions required for learning and memory, which could reduce the effects of A β toxicity on cognitive function *in vivo*.

Generating the 5xFAD-Kif11OE mouse model

In order to investigate the role of KIF11 on the maintenance of cognitive function in AD in an *in vivo* model, we overexpressed mouse Kif11 in the 5xFAD mouse model of AD. The 5xFAD transgenic mouse expresses the human APP gene harboring the “Swedish” double mutation (K670N/M671L), the “Florida” mutation (I716V), and the “London” mutation (V717I), and the human PSEN1 gene harboring the M146L and L286V familial/early onset AD (FAD/EOAD) mutations. Together, these mutations result in the overproduction of A β and the deposition of neuronal A β plaques before six months of age (Bilkei-Gorzo, 2014; Hall and Roberson, 2012; Oakley et al., 2006). The Kif11OE mouse was originally developed to determine whether overexpression of mouse Kif11 leads to genomic instability and cancer (Castillo et al., 2007). In this model, Kif11 overexpression led to mitotic spindle defects, increased genomic instability, higher rates of aneuploidy, and increased tumor development. In addition to these cancer-related phenotypes, Kif11OE mice also exhibit neurological abnormalities, megacystis, and dermatitis. However, the specific neurological phenotypes and effects of Kif11 overexpression on learning and memory have not been examined. By crossing the 5xFAD and Kif11OE strains, we were able to generate double transgenic mice to test whether the ability of Kif11 overexpression to prevent decreases in dendritic spine density caused by A β toxicity leads to a reduction in AD-related cognitive deficits in the 5xFAD mouse model. Additionally, we were able to test whether increased Kif11 expression alone impacts learning and memory by comparing single transgenic Kif11OE mice to their wild-type (WT) littermates.

Kif11OE mice were mated with 5xFAD mice, and the progeny were backcrossed to obtain single and double transgenic mice in a >95% C57Bl/6J genetic background (see STAR methods). This generated litters consisting of non-transgenic WT littermates, single transgenic mice harboring the Kif11OE transgene (Kif11OE), single transgenic mice harboring the 5xFAD transgene (5xFAD), and double transgenic mice harboring both the 5xFAD and Kif11OE transgenes (5xFAD-Kif11OE). To determine whether 5xFAD-Kif11OE mice had altered expression of either the Kif11OE transgene or the 5xFAD transgene, we compared the mRNA expression levels of human *APP* and mouse *Kif11* in whole brain homogenates from 8-month-old mice. We found that both Kif11OE and 5xFAD-Kif11OE mice showed similar levels of *Kif11* overexpression (Figure S3A), and that the 5xFAD and 5xFAD-Kif11OE mice showed similar levels of *APP* overexpression (Figure S3B). These data demonstrate that mating Kif11OE mice successfully produced a viable double transgenic mouse model of AD that overexpresses both mouse *Kif11* and human *APP* at levels similar to those detected in their respective single transgenic littermates.

Increased *Kif11* expression rescues A β -mediated decreases in LTP

Hippocampal LTP has been postulated to be the cellular basis for learning and memory (Bliss and Collingridge, 1993; Roman et al., 1987). As cognitive decline is apparent in AD and in mouse models thereof, including 5xFAD mice, deficits in hippocampal LTP have been attributed to A β toxicity (Crouzin et al., 2013; Kimura and Ohno, 2009). We previously reported that A β -mediated inhibition of *Kif11* is one potential mechanism by which A β inhibits hippocampal LTP (Freund et al., 2016). Because *Kif11* is competitively inhibited by A β (Borysov et al., 2011), we hypothesized that increased *Kif11* expression might help to maintain hippocampal LTP in 5xFAD mice. Specifically, we predicted that *Kif11* overexpression would prevent or reduce A β -mediated deficits in LTP.

As shown in Figure 2, extracellular recordings of synaptic responses measured as the initial slope of the field excitatory postsynaptic potential (fEPSP) at CA1 synapses of 6- to 8-month-old mice revealed that the fEPSP responses were markedly increased in the Kif11OE, WT, and 5xFAD-Kif11OE groups following the induction of LTP by delivery of two high-frequency stimulus (HFS) trains. In contrast to these results, the 5xFAD group fEPSP responses after HFS remained more like baseline responses recorded before HFS (representative traces are shown in Figure 2A), which is consistent with impaired LTP. Accordingly, at 60 min after HFS, the 5xFAD group showed significantly less LTP of the fEPSP response compared to the WT group, whereas the 5xFAD-Kif11OE group showed no significant difference compared to either the WT or Kif11OE groups (Figures 2B and 2C). Our findings reveal that *Kif11* overexpression alone does not affect hippocampal LTP compared to age-matched WT mice, and, more importantly, that *Kif11* overexpression protects against A β -mediated deficits in LTP in 5xFAD mice, as shown in the 5xFAD-Kif11OE mice (Figure 2C). These data align with our previous studies of KIF11 and provide further mechanistic support for the conclusion that A β -mediated inhibition of *Kif11* contributes to cognitive dysfunction in AD. These results also provide evidence that *Kif11* plays a key role in maintaining neuronal functions critical for learning and memory and suggest that increased expression of *Kif11* could reduce cognitive dysfunction in 5xFAD mice despite the presence of A β .

Increased *Kif11* expression rescues spatial and working memory deficits in 6- to 8-month-old 5xFAD mice

Considering the above results in combination with previous studies describing associations with spine density and LTP with cognition (Lynch, 2004; Mahmoud et al., 2015; Penn et al., 2017; Perez-Cruz et al., 2011; Reza-Zaldivar et al., 2020), we wanted to determine whether the observed effects on AD phenotypes (LTP and spine density) by an increase in *Kif11* expression translated into better cognitive performance in our *Kif11*-overexpressing AD mouse model. Here, we focused on the performance of 6- to 8-month-old mice in the radial arm water maze (RAWM) task as a measure of spatial and working memory (Alamed et al., 2006; Arendash et al., 2001; Boyd et al., 2010). The onset of behavioral deficits in 5xFAD mice occurs at approximately five months of age, and the deficits increase with age (Jawhar et al., 2012; Oakley et al., 2006; Richard et al., 2015; Xiao et al., 2015), whereas motor deficits that could potentially confound behavioral testing do not occur until 9–12 months of age (Jawhar et al., 2012; O'Leary et al., 2020; O'Leary et al., 2018). As the RAWM task is motor function-dependent, using this age group allowed us to measure robust effects of A β -induced cognitive deficits before the development of motor deficits in the 5xFAD mice (O'Leary et al., 2020; O'Leary et al., 2018).

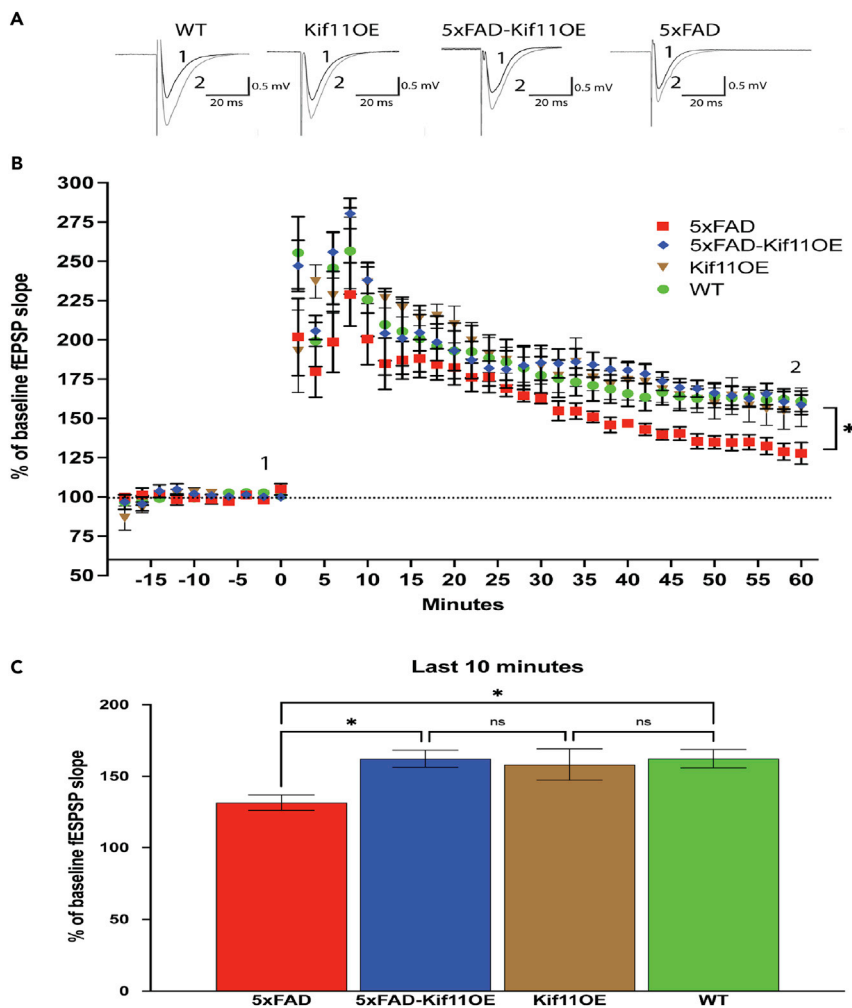


Figure 2. Increased Kif11 expression prevents decreases in early phase long-term potentiation (LTP) in 5xFAD mice

(A) Typical field excitatory post-synaptic potentials (fEPSPs) for each of the four groups of mice (5xFAD, 5xFAD-Kif11OE, Kif11OE, and WT) before (1, gray line) and 60 min after delivery of two 100 Hz, 1 s high-frequency stimulus (HFS) trains delivered 5 min apart to induce LTP (2, black line).

(B) Time course of fEPSP slope measurements (normalized as % of baseline) before and after two HFS trains (black arrows: 1 × 100 Hz each, 5 min apart). Data represent the mean ± SEM for five slices from four animals for the 5xFAD group, six slices from four animals for the 5xFAD-Kif11OE group, and five slices from three animals for the Kif11OE and WT groups.

(C) LTP normalized as % of baseline fEPSP slope at 50–60 min after HFS. Statistically significant differences between groups were determined by ordinary one-way ANOVA with post-hoc Šidák multiple comparison analysis. * $p < 0.05$.

The mice were first placed on the platform to learn its location within the room. The mice were then placed in one of the other five arms of the water maze with the goal of swimming to the location of a submerged platform, using only the environmental cues from the maze and the room (Figure 3A). The ability of the mice to learn the location of the submerged platform and escape the water was measured over two days in 30 trials of testing with 15 trials per day (Figure 3B). To control for the distance of the platform from the point of placement as well as for potential differences in the allocentric and egocentric abilities of the mice, the performance of each mouse was quantified in blocks of trials. The blocks consisted of six trials in the first two blocks of each day and three trials in the last block of each day (Figure 3B), with each trial beginning at a different placement arm (Figure 3B). Profiles of latency time to reach the submerged platform (Figure 3C) revealed that the 5xFAD group performed significantly worse than the WT group ($p < 0.0001$), the Kif11OE group was similar to the WT group, and the double transgenic 5xFAD-Kif11OE group was most similar to the WT group and performed significantly better than the 5xFAD group ($p = 0.0051$).

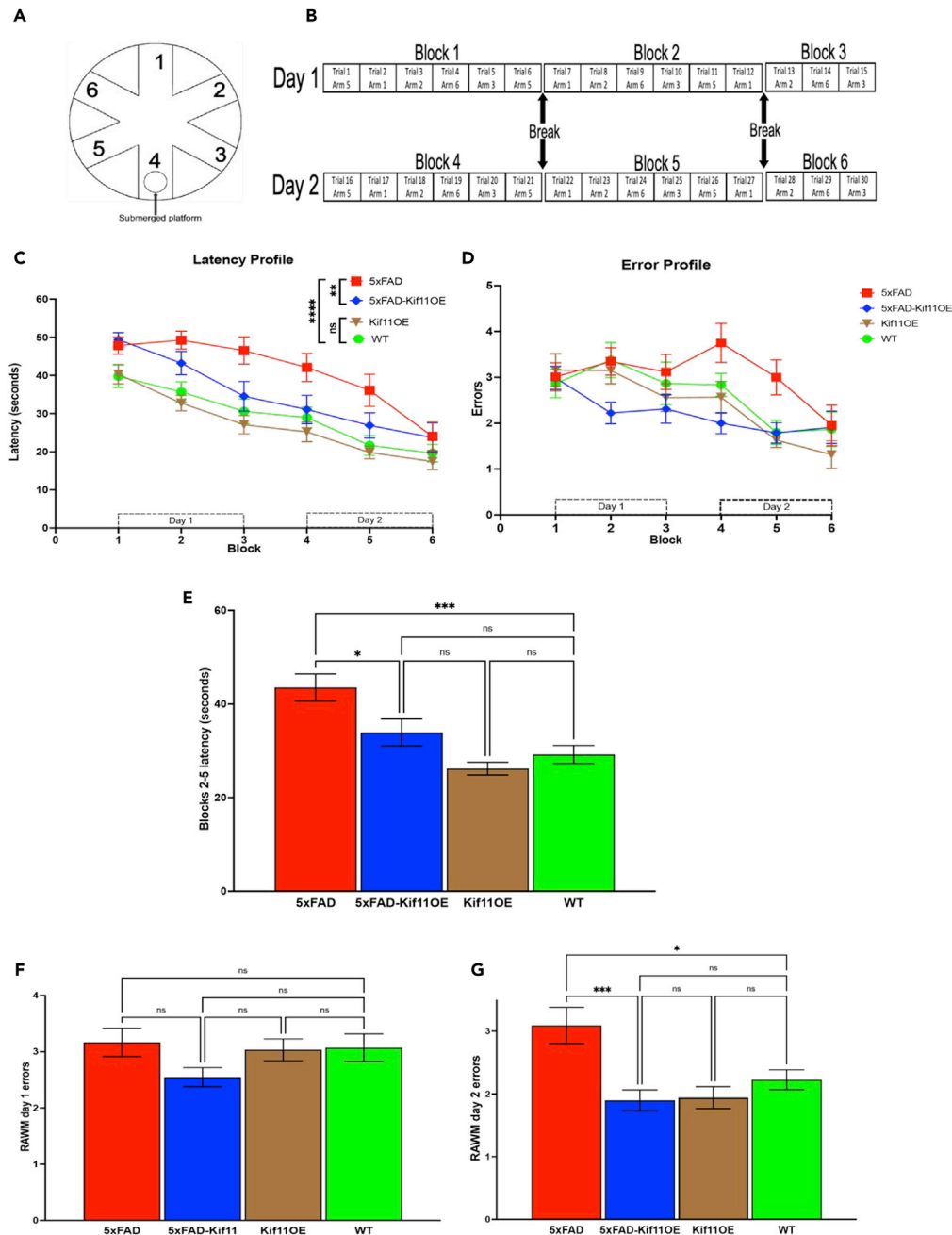


Figure 3. Increased *Kif11* expression rescues working and spatial memory deficits in 6- to 8-month-old 5xFAD mice in the radial arm water maze (RAWM)

(A) Schematic showing the six arms in the RAWM.

(B) Illustration of arm placement and timing of breaks between the 30 trials in the RAWM during two days of testing with 15 trials/day.

(C) Average time per block each group took to find the escape platform.

(D) Average number of errors for each mouse at each block of testing.

(E) Average latency performance in blocks 2-5.

(F) Average errors made by each mouse on day one of testing.

(G) Average errors made by each mouse on day two of testing. 5xFAD, N = 15; 5xFAD-Kif11OE, N = 15; Kif11OE, N = 19; and WT, N = 15. Statistical significance was calculated through ordinary one-way ANOVA with post-hoc Holm-Šidák's multiple comparisons test. Latency and error profiles (C-D) used a general linear model for repeated measures. Data are presented as the mean with error bars representing the SEM. * $p < 0.05$, ** $p < 0.01$, *** $p < 0.001$.

Error profiles of the mice throughout the duration of the testing revealed no significant differences between any of the groups (Figure 3D). Furthermore, quantification and comparison of the average latency in the middle blocks (blocks 2–5) revealed that the 5xFAD mice showed a significantly longer latency compared to WT, Kif11OE, and 5xFAD-Kif11OE mice, and that the latency of 5xFAD-Kif11OE mice was not significantly different from that of WT or Kif11OE mice (Figure 3E). These findings indicate that increased expression of *Kif11* alone does not lead to motor deficits that affect RAWM latency compared to WT mice, and that increased *Kif11* expression leads to decreased RAWM latency in 5xFAD mice to levels similar to those of WT mice. Although there were no significant differences observed in the error profiles of the mice (Figure 3D) or in the average number of errors per block made by any of the four groups during day 1 (Figure 3F), during day 2, the 5xFAD mice made significantly more errors compared to WT, Kif11OE, and 5xFAD-Kif11OE mice (Figure 3G). These findings show that increased expression of *Kif11* reduces the error rate of 5xFAD mice in the RAWM to levels similar to those of WT mice (Figure 3G). The fact that 5xFAD mice made significantly more errors on day 2 of testing, but not on day 1, indicates that 5xFAD mice have deficits in memory-dependent performance that are rescued by increased expression of *Kif11*. Taken together, our results show that increased expression of *Kif11* prevents deficits in learning and memory in the 5xFAD mouse model.

These data, taken together with our cell culture and electrophysiology studies, suggest that *Kif11* plays a key role in maintaining neuronal functions critical for learning and memory, and that the improved performance of the 5xFAD-Kif11OE mice compared to the 5xFAD mice in the RAWM can be attributed, at least in part, to the maintenance of receptor-mediated hippocampal LTP mediated by increased expression of *Kif11*. These data also provide further mechanistic support for the conclusion that A β -mediated inhibition of *Kif11* contributes to cognitive dysfunction in AD.

Increased expression of *Kif11* does not affect brain amyloid deposition in 5xFAD mice

The prevention or reversal of amyloid deposition by active or passive immune therapy against A β , by genetic removal of the gene encoding APOE, which is essential for A β polymerization, or by various immune modulators all lead to cognitive benefits in animal models and in at least some human trials compared to placebo, suggesting the targeting of amyloid as one approach to AD therapy. To test whether the rescue of AD phenotypes that we observed in our behavioral and electrophysiological experiments in 5xFAD-Kif11OE mice might similarly be the result of reduced amyloid deposition, we visualized A β accumulation in different brain regions in 5xFAD, 5xFAD-Kif11OE, and Kif11OE mice using both the NIAD-4 amyloid-binding dye that recognizes beta-sheet structures (Nesterov et al., 2005) and the 6E10 antibody raised against amino acids 1–16 of A β . Histological staining of sagittal slices from 8-month-old mouse brains revealed that both 5xFAD mice (Figure 4A) and 5xFAD-Kif11OE mice (Figure 4B) had robust deposition of amyloid plaques, whereas the Kif11OE mouse had no amyloid signal (Figure 4C). Quantification of the fluorescence-positive area in multiple brain regions revealed that 5xFAD and 5xFAD-Kif11OE mice had similar levels of amyloid plaque burden, and that Kif11OE mice lacked amyloid plaques, based on both NIAD-4 staining (Figure 4D) and 6E10 staining (Figure 4E). Furthermore, whole brain quantification of signal from both NIAD-4 staining and 6E10 staining also revealed similar results, where the 5xFAD and the 5xFAD-Kif11OE mice showed similar levels of amyloid deposition, and the Kif11OE mice lacked amyloid plaques (Figures S4A and S4B). We did not observe any significant differences in DAPI staining in the same brain regions (Figure S5A) or with whole brain quantification of DAPI staining (Figure S5B) in 5xFAD, 5xFAD-Kif11OE, and Kif11OE mice. These data demonstrate that the rescue of learning and memory deficits and the maintenance of LTP in 5xFAD-Kif11OE mice is not due to reduced A β deposition. Instead, increased *Kif11* expression appears to bolster brain function and resiliency by directly improving cellular functions, without decreasing the presence of amyloid deposits in the brain.

Higher brain *KIF11* expression is associated with better cognition in AD patients

The *KIF11* gene has not been directly linked to AD in humans. Although previous genome-wide association studies (GWAS) have identified single nucleotide polymorphisms (SNPs) within the HaploBlock containing *KIF11*, and genomic markers within *KIF11* have shown associations with AD in non-*APOE4* carriers (Feuk et al., 2005), *KIF11*-specific associations with cognitive function have not been reported. The results of our biochemical, cell and tissue culture, and behavioral experiments provide strong evidence that the microtubule motor *KIF11* plays a significant role in A β toxicity, and that this toxicity can be overcome by upregulation of *KIF11* expression. We therefore took the final step to determine whether *KIF11* may

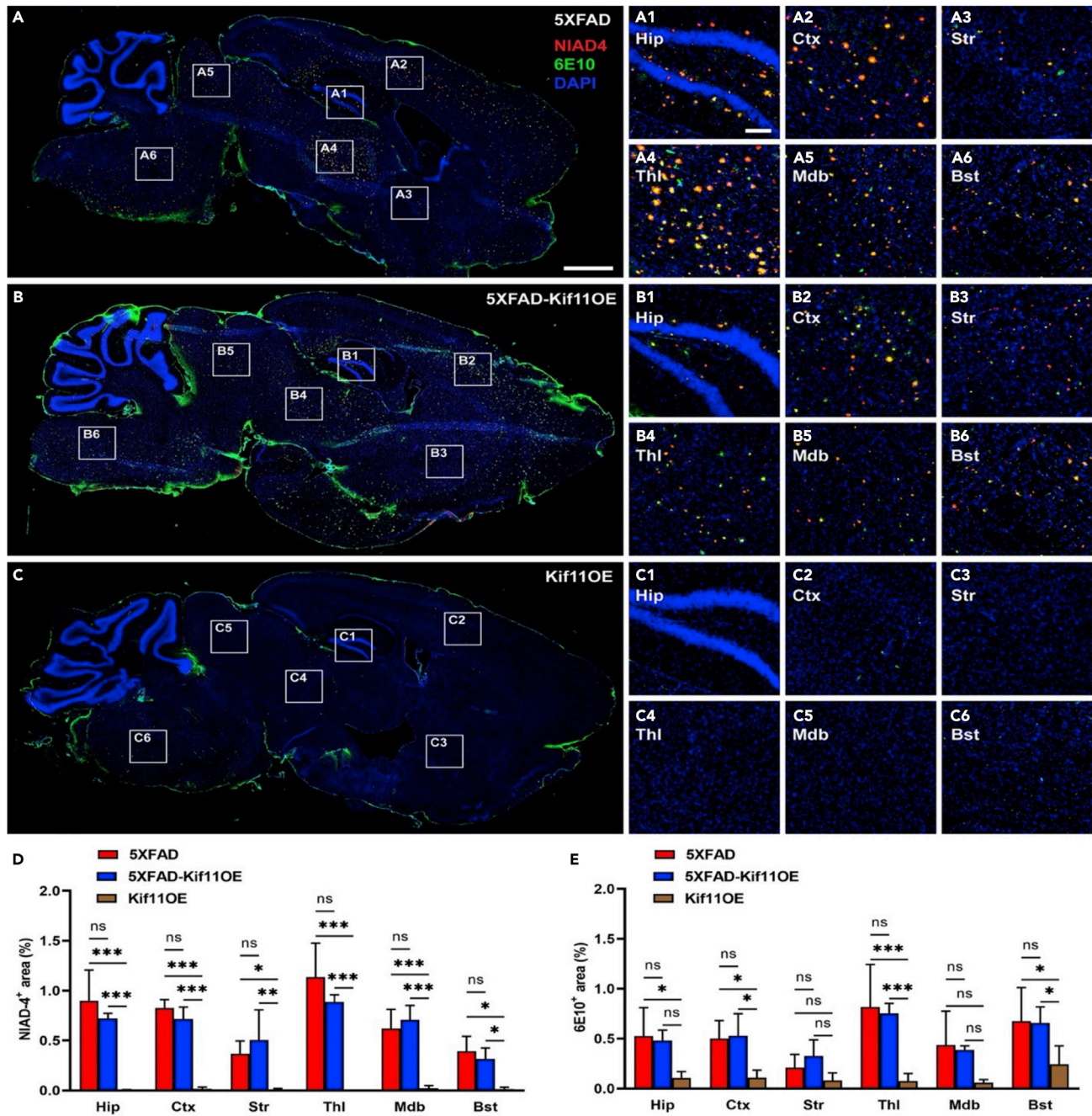


Figure 4. Increased expression of *Kif11* does not reduce amyloid plaques in the brains of 5xFAD mice

Shown are representative images of 20 μm -thick sagittal sections of mouse brain showing areas of the hippocampus (Hip), cortex (Ctx), striatum (Str), thalamus (Thl), midbrain (Mdb), and the brainstem (Bst) that were analyzed to detect amyloid using both NIAD-4 staining (red) and the 6E10 antibody (green) and cell nuclei using DAPI (blue) in 5xFAD (A, A1-A6), 5xFAD-Kif11OE (B, B1-B6), and Kif11OE (C, C1-C6) mice. Quantification of the percent area positive for (D) NIAD-4 staining or (E) 6E10 staining in the different brain regions in 5xFAD, 5xFAD-Kif11OE, and Kif11OE mice. Data represent the mean \pm SD of N = 2–5 slices from three mice in each group. Statistical significance was calculated through ordinary one-way ANOVA with post-hoc Holm-Sidak's multiple comparisons test. Data are presented as the mean with error bars representing the SEM. * $p < 0.05$, ** $p < 0.01$, *** $p < 0.001$.

serve as a key, modifiable target of A β toxicity in human AD patients. We first queried Agora on the publicly available AMP-AD Knowledge Portal [<https://agora.adknowledgeportal.org/genes>; (Hodes and Buckholtz, 2016)] to determine whether there was an association between *KIF11* mRNA expression levels in the cerebellum, frontal pole, inferior frontal gyrus, parahippocampal gyrus, superior temporal gyrus, or

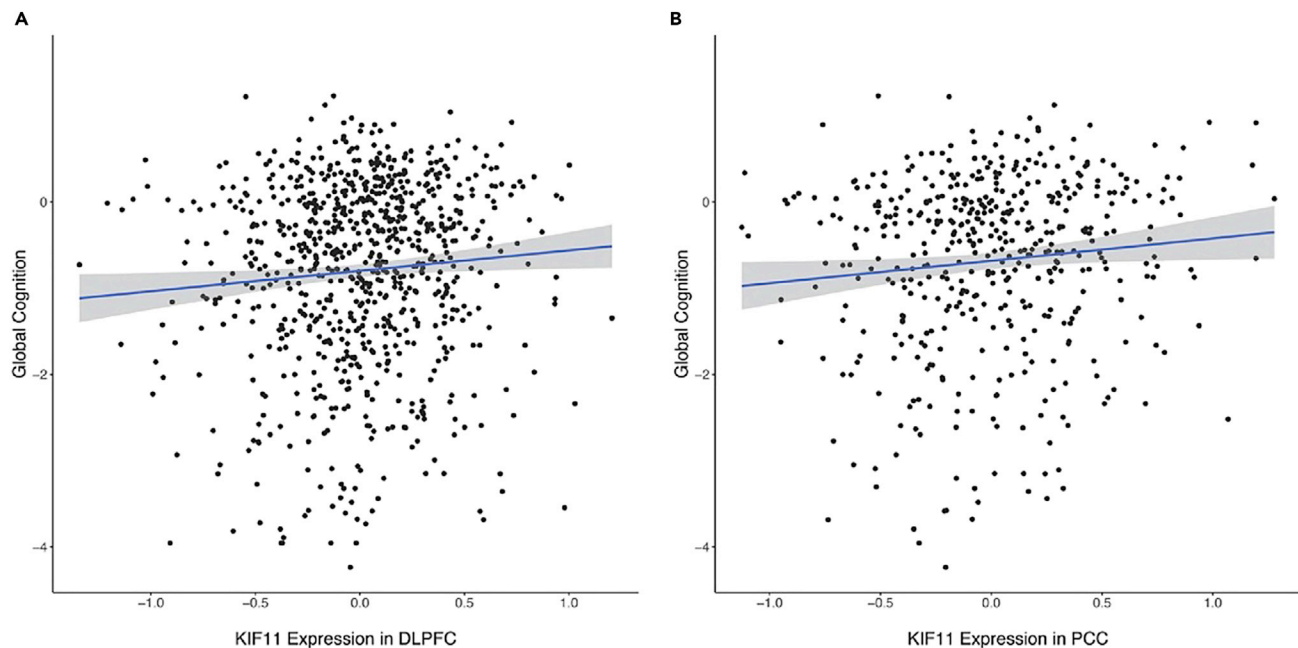


Figure 5. Higher *KIF11* mRNA expression levels in the dorsolateral prefrontal cortex and the posterior cingulate cortex are associated with better cognitive performance

Normalized *KIF11* mRNA expression levels are presented along the xaxis and cognitive performance at the final visit before death is presented along the yaxis. Data from the dorsolateral prefrontal cortex (DLPFC, N = 939 (A) and from the posterior cingulate cortex (PCC, N = 527) (B) showing the correlation between *KIF11* mRNA expression levels and global cognition ($p = 0.03$ for both the DLPFC and the PCC). Shaded areas represent the 95% confidence interval.

the temporal cortex, and a clinical diagnosis of AD, but we did not uncover any correlations (data not shown).

We then assessed whether higher expression of *KIF11* is correlated with cognitive performance by leveraging the deeper phenotypic data from the ROS/MAP study (Bennett et al., 2018). We evaluated associations between *KIF11* mRNA expression levels in three different brain regions, including the DLPFC (N = 939), posterior cingulate cortex (PCC, N = 527), and the head of the caudate nucleus (CN, N = 715), and cognitive performance using previously described STAR methods (Moore et al., 2020), which are described in the STAR Methods. In the two cortical regions, including the DLPFC and PCC, we observed an association between higher levels of *KIF11* mRNA expression in the DLPFC (Figure 5A; $\beta = 0.21$, $p = 0.03$) and in the PCC (Figure 5B; $\beta = 0.25$, $p = 0.03$) and better cognitive performance at the final visit before death, but we did not observe a similar association in the CN ($\beta = 0.05$, $p = 0.63$). The same association was also observed in longitudinal analyses, but only in the DLPFC ($\beta = 0.02$, $p = 0.03$), whereas no association was present in the PCC or CN ($p > 0.25$).

To determine whether expression of *KIF11* mRNA in the DLPFC of ROS/MAP participants as detected by RNAseq was cell type specific, we assessed expression from a previously published snRNA sequencing dataset quantified leveraging postmortem prefrontal cortex tissue from 48 participants in ROS/MAP (Mathys et al., 2019). In agreement with a previous report showing that *KIF11* is expressed in mature neurons (Lin et al., 2011), as well as the cell type expression of *KIF11* in the human brain as described by the Human Protein Atlas (Uhlen et al., 2015), we found that the expression of *KIF11* in the brains of ROS/MAP participants was not particularly robust, but the *KIF11* mRNA signal observed was primarily due to its expression in both excitatory and inhibitory neurons (Figure S6). Additionally, we assessed the degree to which the observed expression of *KIF11* in the bulk tissue leveraged for our primary analysis correlated with the proportions of different cell types within that sample. Cellular fractions were estimated leveraging a previously published multi-marker deconvolution algorithm that estimates the proportion of excitatory neurons, inhibitory neurons, astrocytes, microglia, oligodendrocytes, oligodendrocyte progenitor cells, and endothelial pericytes based on the transcriptomic signature (Cain et al., 2022). Indeed, *KIF11* expression levels were positively

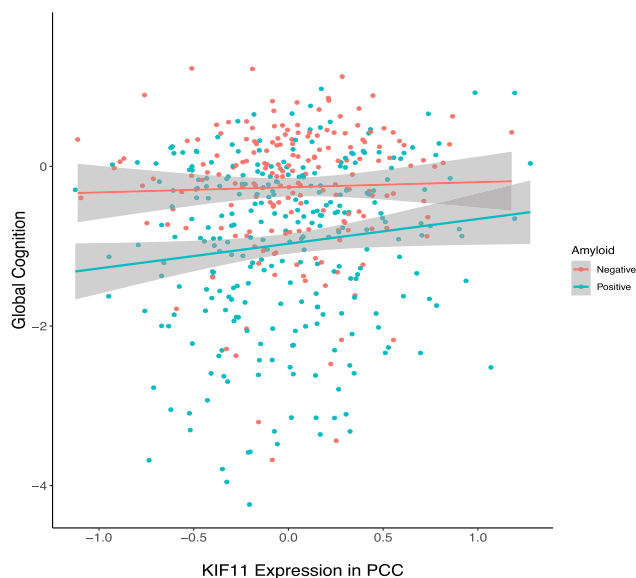


Figure 6. Higher *KIF11* mRNA expression levels in the posterior cingulate cortex are associated with better cognitive performance in neuritic plaque-positive individuals, but not in neuritic plaque-negative individuals

KIF11 mRNA expression levels in the posterior cingulate cortex (PCC, N = 527) are presented along the xaxis, and cognitive performance at the final visit before death is presented along the yaxis. Points and lines are colored based on neuritic plaque positivity where neuritic plaque-positive individuals are shown in blue (CERAD \geq moderate; $p = 0.04$), and neuritic plaque-negative individuals are shown in red (CERAD < moderate; $p = 0.36$). Shaded areas represent the 95% confidence interval.

correlated with the proportion of excitatory and inhibitory neurons in the DLPFC, and negatively correlated with the proportion of astrocytes, microglia, oligodendrocytes, oligodendrocyte progenitor cells, and endothelial pericytes in the DLPFC (Figure S6).

Finally, based on the results of our AD mouse and cell studies showing that *KIF11* overexpression protects against the consequences of amyloidosis, we also evaluated whether associations between *KIF11* expression and cognition were particularly strong among individuals with neuritic plaque pathology at autopsy. We first examined the statistical interaction between *KIF11* expression levels and neuritic plaque pathology, but we did not observe a statistically significant interaction in any brain region ($p > 0.28$), which limited our ability to speak to differences by neuropathological stage. However, in exploratory follow-up stratified analyses, the association between higher *KIF11* mRNA expression in the PCC and cognitive performance was present among those with moderate or frequent neuritic plaque pathology at autopsy (Figure 6; $\beta = 0.31$, $p = 0.04$), but not among those with sparse or no neuritic plaques at autopsy ($\beta = 0.12$, $p = 0.36$). A similar pattern was observed in the DLPFC, although results in neuritic plaque-positive participants were marginally non-significant ($p = 0.06$). These data indicate that cortical *KIF11* expression is positively correlated with cognition in AD patients and is consistent with the results of our studies in 5xFAD mice in which increased *Kif11* expression had a significant protective effect against learning and memory deficits (Figure 3) and against A β -mediated decreases in LTP (Figure 2).

DISCUSSION

Many current experimental treatments for AD have focused on reducing A β production or on increasing the clearance of A β plaques [reviewed in (Demattos et al., 2012; Imbimbo and Watling, 2019; Jeremic et al., 2021)]. Most of these approaches have failed to prevent or reverse cognitive decline in clinical trials, although one such anti-A β human monoclonal antibody drug (aducanumab/Aduhelm) may modestly slow cognitive decline compared to placebo (Cummings et al., 2014, 2020; Graham et al., 2017). Clearly, alternative approaches to the development of AD therapeutics are needed. Our *in vitro* and *in vivo* experiments using animal and cell models of AD together with analyses of human AD patient data show that the

KIF11 microtubule motor protein plays a key role in the maintenance of cognitive function and demonstrate that A β -mediated inhibition of KIF11 leads to the cognitive deficits that occur during AD pathogenesis. Specifically, our behavioral and electrophysiological experiments show that increased *Kif11* expression overrides the inhibitory effects of A β , thereby preserving LTP and improving cognitive performance. Our previous biochemical experiments showed that the mechanism by which increased *Kif11* expression overcomes the damaging effects of A β likely derives from protecting the enzymatic activity of this important microtubule motor protein from complete inhibition by A β to preserve its many cytoskeletal functions that are required for the localization of neurotransmitter and neurotrophin receptors to their functional location on the plasma membrane where they regulate neuronal morphology, including maintaining the correct number of neurotransmitter-harboring dendritic spines, which has been previously hypothesized to serve as a marker of cognitive resilience in AD (Boros et al., 2017; Walker and Herskowitz, 2020). Our finding that *Kif11* overexpression does not affect A β production or deposition in 5xFAD mice shows that the beneficial effects of *Kif11* overexpression on cognition and LTP in our 5xFAD-Kif11OE mice occurred despite the persistence of amyloid plaques and pathology in the brains of these mice and reinforces the conclusion that the enzymatic function of KIF11 is inhibited by A β and can be recovered by KIF11 overexpression.

Although statistically significant, the associations between *KIF11* expression levels and cognitive performance in ROS/MAP study participants are modest. Evidently, in human populations, increased endogenous levels of *KIF11* mRNA are not sufficient to prevent AD, nor do they fully out-compete environmental or genetic factors that may enhance susceptibility to AD. However, our results suggest that higher *KIF11* expression levels may partially prevent cognitive loss during the course of AD, which aligns with our previous findings regarding the role of KIF11 in animal models of AD (Ari et al., 2014; Borysov et al., 2011; Freund et al., 2016). Indeed, further analyses of human AD study data is needed to fully elucidate the role of *KIF11* in AD resilience or susceptibility, as well as the environmental factors that may regulate *KIF11* expression or function, which could lead to the development of an entirely new approach to AD therapy.

Our data and experimental models show the importance of KIF11 function for maintaining cognitive function and synaptic plasticity in the presence of A β and elucidate the potential for novel AD therapeutic strategies that target A β toxicity based on enhancing KIF11 activity. In particular, we propose that overriding the toxic effects of A β by either increasing *Kif11* mRNA expression levels or by blocking A β -mediated inhibition of KIF11 may be a viable therapeutic strategy for the treatment of AD.

As a whole, the data we present herein further highlight the importance of KIF11 in learning and memory and the possibility of developing therapies for AD that focus on maintaining neuronal structures and functions by targeting molecules that regulate microtubule dynamics, stability, and transport capability. Although chemical compounds that alter microtubule dynamics were investigated previously as a potential therapy for AD (Brunden et al., 2010, 2014; Zhang et al., 2012), our new data demonstrate the potential utility of focusing on a microtubule motor protein inhibited by A β , specifically KIF11, and its increased expression and/or activity as a potential therapeutic target for AD. To our knowledge, there have been no other *in vivo* studies showing that increased expression of a gene such as *KIF11*, whose protein product is inhibited by A β and is involved in regulating microtubule dynamics and organization and localizing receptors on neurons, offsets the cognitive deficits caused by A β . Thus, our findings illustrate the potential efficacy of a new approach to AD therapy that involves overriding or blocking the inhibitory effects of A β on a specific cellular protein.

It is of interest to note that in addition to A β , excess tau protein has been shown to inhibit *Kif11* and consequently cause the cell cycle defects, chromosome mis-segregation, neuronal aneuploidy, and apoptosis that characterize a *Drosophila* model of frontotemporal dementia (FTD, also termed frontotemporal lobar degeneration, FTL) (Bougé and Parmentier, 2016; Malmanche et al., 2017). Such microtubule-dependent cell cycle defects, which lead to neuronal aneuploidy and apoptosis, have also been observed in human FTD/FTLD caused by mutations in the gene encoding tau [MAPT; (Canes et al., 2018); for discussion, see (Potter et al., 2019)]. Thus, two of the major pathological and biochemical features of AD — A β and tau — both inhibit KIF11 activity and function, further supporting our conclusion that KIF11 is a key component in the AD pathogenic pathway that may hold

promise as a future target for therapeutic drug development efforts, with potential applicability to other neurodegenerative diseases.

Limitations of the study

Using cell culture and mouse model systems for AD in addition to analysis of gene expression in the DLPFC of humans, this study demonstrated that increased *KIF11/Kinesin-5* expression prevented A β -mediated cognitive loss. However, our study is not without limitations. Our behavioral assay in mouse models focused on a specific age range (6–8 months of age), and therefore the extent to which increased *Kif11* expression offsets cognitive loss in 5xFAD mice as they age has not yet been elucidated. Additionally, our investigations using mice are limited to and focused on cognitive loss due to A β -mediated toxicity. Because AD phenotypes in humans and in some AD model systems include excess tau, which has also been shown to inhibit the Kinesin-5 motor protein (Bougé and Parmentier, 2016), a model system that includes both tau and A β pathology with specificity to AD would be needed to determine the effects of KIF11 expression on tau-mediated AD phenotypes.

STAR★METHODS

Detailed methods are provided in the online version of this paper and include the following:

- KEY RESOURCES TABLE
- RESOURCE AVAILABILITY
 - Lead contact
 - Resource availability
 - Data and code availability
- EXPERIMENTAL MODEL AND SUBJECT DETAILS
 - Animals
 - Primary neuron cultures
 - Human
- METHOD DETAILS
 - Genotyping of transgenic mouse lines
 - Gene expression analyses
 - Radial arm water maze (RAWM)
 - Electrophysiology
 - Neuronal cultures
 - Mouse brain collection and amyloid staining
 - ROS/MAP study analyses
- QUANTIFICATION AND STATISTICAL ANALYSIS

SUPPLEMENTAL INFORMATION

Supplemental information can be found online at <https://doi.org/10.1016/j.isci.2022.105288>.

ACKNOWLEDGMENTS

We would like to thank Dr. Jennifer Sanderson for help in preparing for the electrophysiology experiments. Additionally, we would like to thank Neil Markham for his mentorship, contributions, and help in the maintenance of our mouse colony and Vanesa Adame for her help and contributions to the behavioral studies presented here. We thank the CU Anschutz Neurotechnology Center Animal Behavior Core staff, specifically Drs. Michael Mesches and Nicolas Busquet, for their help and contributions to the mouse behavior studies. Finally, we would thank entire staff of the CU Anschutz Office of Live Animal Research for their care and maintenance of our mouse colonies. The graphical abstract presented in this manuscript was created with BioRender ([biorender.com](https://www.biorender.com)). This work was supported by NIH grants F99NS115330 to E.M.L., R01NS110383 to M.L.D., K01AG049164, R01AG059716, and R01AG061518 to T.J.H., and P30AG10161 and P30AG72975 (ROS), R01AG15819 (ROSMAP; genomics and RNAseq), and R01AG17917 (MAP), and U01AG61356 (ROSMAP) to D.A.B., as well as gift funds from the University of Colorado Alzheimer's and Cognition Center to H.P. Additional phenotypic data from Rush can be requested at www.radc.rush.edu and additional data can be requested from the AD Knowledge Portal (<https://adknowledgeportal.synapse.org>) and Rush Alzheimer's Disease Center Resource Sharing Hub (<https://www.radc.rush.edu>).

AUTHOR CONTRIBUTIONS

Conceptualization: E.M.L., H.J.C., and H.P.; Behavioral assays and data analyses: E.M.L. and M.M.A.; Electrophysiology execution and data analyses: E.M.L., R.K.F., M.D.A., and O.P.; Cell culture experiments and data analyses: E.S. and M.D.A. Immunohistochemistry: B.D., N.R.J., and E.M.L.; Generation and access to ROSMAP data: D.A.B.; Analysis of ROSMAP data: T.J.H., A.S., and E.M.L.; This manuscript was prepared by E.M.L. under the co-mentorship of H.J.C. and H.P. All authors provided edits to this manuscript and have approved of the final version.

DECLARATION OF INTERESTS

The authors have no financial conflicts of interest.

INCLUSION AND DIVERSITY

One or more of the authors of this paper self-identifies as an underrepresented ethnic minority in their field of research or within their geographical location. One or more of the authors of this paper self-identifies as a gender minority in their field of research. One or more of the authors of this paper self-identifies as a member of the LGBTQ+ community. One or more of the authors of this paper received support from a program designed to increase minority representation in their field of research.

Received: February 28, 2022

Revised: August 8, 2022

Accepted: October 4, 2022

Published: November 18, 2022

REFERENCES

- Alamed, J., Wilcock, D.M., Diamond, D.M., Gordon, M.N., and Morgan, D. (2006). Two-day radial-arm water maze learning and memory task; robust resolution of amyloid-related memory deficits in transgenic mice. *Nat. Protoc.* *1*, 1671–1679. <https://doi.org/10.1038/nprot.2006.275>.
- Arendash, G.W., King, D.L., Gordon, M.N., Morgan, D., Hatcher, J.M., Hope, C.E., and Diamond, D.M. (2001). Progressive, age-related behavioral impairments in transgenic mice carrying both mutant amyloid precursor protein and presenilin-1 transgenes. *Brain Res.* *891*, 42–53. [https://doi.org/10.1016/S0006-8993\(00\)03186-3](https://doi.org/10.1016/S0006-8993(00)03186-3).
- Ari, C., Borysov, S.I., Wu, J., Padmanabhan, J., and Potter, H. (2014). Alzheimer amyloid beta inhibition of Eg5/kinesin 5 reduces neurotrophin and/or transmitter receptor function. *Neurobiol. Aging* *35*, 1839–1849. <https://doi.org/10.1016/j.neurobiolaging.2014.02.006>.
- Bartoli, K.M., Jakovljevic, J., Woolford, J.L., Jr., and Saunders, W.S. (2011). Kinesin molecular motor Eg5 functions during polypeptide synthesis. *Mol. Biol. Cell* *22*, 3420–3430. <https://doi.org/10.1091/mbc.E11-03-0211>.
- Bennett, D.A., Buchman, A.S., Boyle, P.A., Barnes, L.L., Wilson, R.S., and Schneider, J.A. (2018). Religious orders study and rush memory and aging Project. *J. Alzheimers Dis.* *64*, S161–S189. <https://doi.org/10.3233/JAD-179939>.
- Bennett, D.A., Schneider, J.A., Arvanitakis, Z., and Wilson, R.S. (2012a). Overview and findings from the religious orders study. *Curr. Alzheimer Res.* *9*, 628–645. <https://doi.org/10.2174/156720512801322573>.
- Bennett, D.A., Schneider, J.A., Buchman, A.S., Barnes, L.L., Boyle, P.A., and Wilson, R.S. (2012b). Overview and findings from the rush memory and aging Project. *Curr. Alzheimer Res.* *9*, 646–663. <https://doi.org/10.2174/156720512801322663>.
- Bilkei-Gorzo, A. (2014). Genetic mouse models of brain ageing and Alzheimer's disease. *Pharmacol. Ther.* *142*, 244–257. <https://doi.org/10.1016/j.pharmthera.2013.12.009>.
- Blangy, A., Lane, H.A., d'Hérin, P., Harper, M., Kress, M., and Nigg, E.A. (1995). Phosphorylation by p34cdc2 regulates spindle association of human Eg5, a kinesin-related motor essential for bipolar spindle formation in vivo. *Cell* *83*, 1159–1169. [https://doi.org/10.1016/0092-8674\(95\)90142-6](https://doi.org/10.1016/0092-8674(95)90142-6).
- Bliss, T.V., and Collingridge, G.L. (1993). A synaptic model of memory: long-term potentiation in the hippocampus. *Nature* *361*, 31–39. <https://doi.org/10.1038/361031a0>.
- Bodrug, T., Wilson-Kubalek, E.M., Nithianantham, S., Thompson, A.F., Alfieri, A., Gaska, I., Major, J., Debs, G., Inagaki, S., Gutierrez, P., et al. (2020). The kinesin-5 tail domain directly modulates the mechanochemical cycle of the motor domain for anti-parallel microtubule sliding. *Elife* *9*, e51131. <https://doi.org/10.7554/eLife.51131>.
- Boros, B.D., Greathouse, K.M., Gentry, E.G., Curtis, K.A., Birchall, E.L., Gearing, M., and Herskowitz, J.H. (2017). Dendritic spines provide cognitive resilience against Alzheimer's disease. *Ann. Neurol.* *82*, 602–614. <https://doi.org/10.1002/ana.25049>.
- Borysov, S.I., Granic, A., Padmanabhan, J., Walczak, C.E., and Potter, H. (2011). Alzheimer Abeta disrupts the mitotic spindle and directly inhibits mitotic microtubule motors. *Cell Cycle* *10*, 1397–1410. <https://doi.org/10.4161/cc.10.9.15478>.
- Bougé, A.L., and Parmentier, M.L. (2016). Tau excess impairs mitosis and kinesin-5 function, leading to aneuploidy and cell death. *Dis. Model. Mech.* *9*, 307–319. <https://doi.org/10.1242/dmm.022558>.
- Boyd, T.D., Bennett, S.P., Mori, T., Governatori, N., Runfeldt, M., Norden, M., Padmanabhan, J., Neame, P., Wefes, I., Sanchez-Ramos, J., et al. (2010). GM-CSF upregulated in rheumatoid arthritis reverses cognitive impairment and amyloidosis in Alzheimer mice. *J. Alzheimers Dis.* *21*, 507–518. <https://doi.org/10.3233/JAD-2010-091471>.
- Brunden, K.R., Trojanowski, J.Q., Smith, A.B., 3rd, Lee, V.M.Y., and Ballatore, C. (2014). Microtubule-stabilizing agents as potential therapeutics for neurodegenerative disease. *Bioorg. Med. Chem.* *22*, 5040–5049. <https://doi.org/10.1016/j.bmc.2013.12.046>.
- Brunden, K.R., Zhang, B., Carroll, J., Yao, Y., Potuzak, J.S., Hogan, A.M.L., Iba, M., James, M.J., Xie, S.X., Ballatore, C., et al. (2010). Epothilone D improves microtubule density, axonal integrity, and cognition in a transgenic mouse model of tauopathy. *J. Neurosci.* *30*, 13861–13866. <https://doi.org/10.1523/JNEUROSCI.3059-10.2010>.
- Cain, A., Taga, M., McCabe, C., Green, G., Hekselman, I., White, C.C., Lee, D.I., Gaur, P., Rozenblatt-Rosen, O., Zhang, F., et al. (2022). Multi-cellular communities are perturbed in the aging human brain and Alzheimer's disease. Preprint at bioRxiv. <https://doi.org/10.1101/2020.12.22.424084>.
- Caneus, J., Granic, A., Rademakers, R., Dickson, D.W., Coughlan, C.M., Chial, H.J., and Potter, H.

- (2018). Mitotic defects lead to neuronal aneuploidy and apoptosis in frontotemporal lobar degeneration caused by MAPT mutations. *Mol. Biol. Cell* 29, 575–586. <https://doi.org/10.1091/mbc.E17-01-0031>.
- Castillo, A., Morse, H.C., 3rd, Godfrey, V.L., Naeem, R., and Justice, M.J. (2007). Overexpression of Eg5 causes genomic instability and tumor formation in mice. *Cancer Res.* 67, 10138–10147. <https://doi.org/10.1158/0008-5472.CAN-07-0326>.
- Chen, Y., and Hancock, W.O. (2015). Kinesin-5 is a microtubule polymerase. *Nat. Commun.* 6, 8160. <https://doi.org/10.1038/ncomms9160>.
- Crouzin, N., Baranger, K., Cavalier, M., Marchalant, Y., Cohen-Solal, C., Roman, F.S., Khrestchatsky, M., Rivera, S., Féron, F., and Vignes, M. (2013). Area-specific alterations of synaptic plasticity in the 5XFAD mouse model of Alzheimer's disease: dissociation between somatosensory cortex and hippocampus. *PLoS One* 8, e74667. <https://doi.org/10.1371/journal.pone.0074667>.
- Cummings, J., Lee, G., Ritter, A., Sabbagh, M., and Zhong, K. (2020). Alzheimer's disease drug development pipeline: 2020. *Alzheimers Dement.* 6, e12050. <https://doi.org/10.1002/trc2.12050>.
- Cummings, J.L., Morstorf, T., and Zhong, K. (2014). Alzheimer's disease drug-development pipeline: few candidates, frequent failures. *Alzheimer's Res. Ther.* 6, 37. <https://doi.org/10.1186/alzrt269>.
- DeKosky, S.T., and Scheff, S.W. (1990). Synapse loss in frontal cortex biopsies in Alzheimer's disease: correlation with cognitive severity. *Ann. Neurol.* 27, 457–464. <https://doi.org/10.1002/ana.410270502>.
- Demattos, R.B., Lu, J., Tang, Y., Racke, M.M., Delong, C.A., Tzaferis, J.A., Hole, J.T., Forster, B.M., McDonnell, P.C., Liu, F., et al. (2012). A plaque-specific antibody clears existing beta-amyloid plaques in Alzheimer's disease mice. *Neuron* 76, 908–920. <https://doi.org/10.1016/j.neuron.2012.10.029>.
- Dent, E.W. (2017). Of microtubules and memory: implications for microtubule dynamics in dendrites and spines. *Mol. Biol. Cell* 28, 1–8. <https://doi.org/10.1091/mbc.E15-11-0769>.
- Falnikar, A., Tole, S., and Baas, P.W. (2011). Kinesin-5, a mitotic microtubule-associated motor protein, modulates neuronal migration. *Mol. Biol. Cell* 22, 1561–1574. <https://doi.org/10.1091/mbc.E10-11-0905>.
- Ferenz, N.P., Gable, A., and Wadsworth, P. (2010). Mitotic functions of kinesin-5. *Semin. Cell Dev. Biol.* 21, 255–259. <https://doi.org/10.1016/j.semcdb.2010.01.019>.
- Ferhat, L., Cook, C., Chauviere, M., Harper, M., Kress, M., Lyons, G.E., and Baas, P.W. (1998). Expression of the mitotic motor protein Eg5 in postmitotic neurons: implications for neuronal development. *J. Neurosci.* 18, 7822–7835.
- Fernandez-Valenzuela, J.J., Sanchez-Varo, R., Muñoz-Castro, C., De Castro, V., Sanchez-Mejias, E., Navarro, V., Jimenez, S., Nuñez-Díaz, C., Gomez-Arboledas, A., Moreno-Gonzalez, I., et al. (2020). Enhancing microtubule stabilization rescues cognitive deficits and ameliorates pathological phenotype in an amyloidogenic Alzheimer's disease model. *Sci. Rep.* 10, 14776. <https://doi.org/10.1038/s41598-020-71767-4>.
- Feuk, L., McCarthy, S., Andersson, B., Prince, J.A., and Brookes, A.J. (2005). Mutation screening of a haplotype block around the insulin degrading enzyme gene and association with Alzheimer's disease. *Am. J. Med. Genet. B Neuropsychiatr. Genet.* 136B, 69–71. <https://doi.org/10.1002/ajmg.b.30172>.
- Freixo, F., Martinez Delgado, P., Manso, Y., Sánchez-Huertas, C., Lacasa, C., Soriano, E., Roig, J., and Lüders, J. (2018). NEK7 regulates dendrite morphogenesis in neurons via Eg5-dependent microtubule stabilization. *Nat. Commun.* 9, 2330. <https://doi.org/10.1038/s41467-018-04706-7>.
- Freund, R.K., Gibson, E.S., Potter, H., and Dell'Acqua, M.L. (2016). Inhibition of the motor protein Eg5/kinesin-5 in amyloid beta-mediated impairment of hippocampal long-term potentiation and dendritic spine loss. *Mol. Pharmacol.* 89, 552–559. <https://doi.org/10.1124/mol.115.103085>.
- Geller, L.N., and Potter, H. (1999). Chromosome missegregation and trisomy 21 mosaicism in Alzheimer's disease. *Neurobiol. Dis.* 6, 167–179. <https://doi.org/10.1006/nbdi.1999.0236>.
- Golovayashkina, N., Penazzi, L., Ballatore, C., Smith, A.B., 3rd, Bakota, L., and Brandt, R. (2015). Region-specific dendritic simplification induced by Abeta, mediated by tau via dysregulation of microtubule dynamics: a mechanistic distinct event from other neurodegenerative processes. *Mol. Neurodegener.* 10, 60. <https://doi.org/10.1186/s13024-015-0049-0>.
- Graham, W.V., Bonito-Oliva, A., and Sakmar, T.P. (2017). Update on Alzheimer's disease therapy and prevention strategies. *Annu. Rev. Med.* 68, 413–430. <https://doi.org/10.1146/annurev-med-042915-103753>.
- Hall, A.M., and Roberson, E.D. (2012). Mouse models of Alzheimer's disease. *Brain Res. Bull.* 88, 3–12. <https://doi.org/10.1016/j.brainresbull.2011.11.017>.
- Hardy, J.A., and Higgins, G.A. (1992). Alzheimer's disease: the amyloid cascade hypothesis. *Science* 256, 184–185. <https://doi.org/10.1126/science.1566067>.
- Hodes, R.J., and Buckholtz, N. (2016). Accelerating Medicines partnership: Alzheimer's disease (AMP-AD) knowledge portal Aids Alzheimer's drug discovery through open data sharing. *Expert Opin. Ther. Targets* 20, 389–391. <https://doi.org/10.1517/14728222.2016.1135132>.
- Hsieh, H., Boehm, J., Sato, C., Iwatsubo, T., Tomita, T., Sisodia, S., and Malinow, R. (2006). AMPAR removal underlies Abeta-induced synaptic depression and dendritic spine loss. *Neuron* 52, 831–843. <https://doi.org/10.1016/j.neuron.2006.10.035>.
- Imbimbo, B.P., and Watling, M. (2019). Investigational BACE inhibitors for the treatment of Alzheimer's disease. *Expert Opin. Invest. Drugs* 28, 967–975. <https://doi.org/10.1080/13543784.2019.1683160>.
- Ingelsson, M., Fukumoto, H., Newell, K.L., Growdon, J.H., Hedley-Whyte, E.T., Frosch, M.P., Albert, M.S., Hyman, B.T., and Irizarry, M.C. (2004). Early Abeta accumulation and progressive synaptic loss, gliosis, and tangle formation in AD brain. *Neurology* 62, 925–931. <https://doi.org/10.1212/01.wnl.0000115115.98960.37>.
- Jawhar, S., Trawicka, A., Jenneckens, C., Bayer, T.A., and Wirths, O. (2012). Motor deficits, neuron loss, and reduced anxiety coinciding with axonal degeneration and intraneuronal Abeta aggregation in the 5XFAD mouse model of Alzheimer's disease. *Neurobiol. Aging* 33, 196.e29–e40. <https://doi.org/10.1016/j.neurobiolaging.2010.05.027>.
- Jeremic, D., Jiménez-Díaz, L., and Navarro-López, J.D. (2021). Past, present and future of therapeutic strategies against amyloid-beta peptides in Alzheimer's disease: a systematic review. *Ageing Res. Rev.* 72, 101496. <https://doi.org/10.1016/j.arr.2021.101496>.
- Kahn, O.I., Ha, N., Baird, M.A., Davidson, M.W., and Baas, P.W. (2015a). TPX2 regulates neuronal morphology through kinesin-5 interaction. *Cytoskeleton (Hoboken)* 72, 340–348. <https://doi.org/10.1002/cm.21234>.
- Kahn, O.I., Sharma, V., González-Billault, C., and Baas, P.W. (2015b). Effects of kinesin-5 inhibition on dendritic architecture and microtubule organization. *Mol. Biol. Cell* 26, 66–77. <https://doi.org/10.1091/mbc.E14-08-1313>.
- Kapitein, L.C., Peterman, E.J.G., Kwok, B.H., Kim, J.H., Kapoor, T.M., and Schmidt, C.F. (2005). The bipolar mitotic kinesin Eg5 moves on both microtubules that it crosslinks. *Nature* 435, 114–118. <https://doi.org/10.1038/nature03503>.
- Kimura, R., and Ohno, M. (2009). Impairments in remote memory stabilization precede hippocampal synaptic and cognitive failures in 5XFAD Alzheimer mouse model. *Neurobiol. Dis.* 33, 229–235. <https://doi.org/10.1016/j.nbd.2008.10.006>.
- Lim, A.S.P., Srivastava, G.P., Yu, L., Chibnik, L.B., Xu, J., Buchman, A.S., Schneider, J.A., Myers, A.J., Bennett, D.A., and De Jager, P.L. (2014). 24-hour rhythms of DNA methylation and their relation with rhythms of RNA expression in the human dorsolateral prefrontal cortex. *PLoS Genet.* 10, e1004792. <https://doi.org/10.1371/journal.pgen.1004792>.
- Lin, S., Liu, M., Son, Y.J., Timothy Himes, B., Snow, D.M., Yu, W., and Baas, P.W. (2011). Inhibition of Kinesin-5, a microtubule-based motor protein, as a strategy for enhancing regeneration of adult axons. *Traffic* 12, 269–286. <https://doi.org/10.1111/j.1600-0854.2010.01152.x>.
- Logsdon, B.A., Perumal, T.M., Swarup, V., Wang, M., Funk, C., Gaiteri, C., Allen, M., Wang, X., Dammer, E., Srivastava, G., et al. (2019). Meta-analysis of the human brain transcriptome identifies heterogeneity across human AD coexpression modules robust to sample collection and methodological approach. Preprint at bioRxiv. <https://doi.org/10.1101/510420>.
- Lynch, M.A. (2004). Long-term potentiation and memory. *Physiol. Rev.* 84, 87–136. <https://doi.org/10.1152/physrev.00014.2003>.

- Mahmoud, R.R., Sase, S., Aher, Y.D., Sase, A., Gröger, M., Mokhtar, M., Höger, H., and Lubec, G. (2015). Spatial and working memory is linked to spine density and mushroom spines. *PLoS One* 10, e0139739. <https://doi.org/10.1371/journal.pone.0139739>.
- Malmanche, N., Dourlen, P., Gistelincq, M., Demiautte, F., Link, N., Dupont, C., Vanden Broeck, L., Werkmeister, E., Amouyel, P., Bongiovanni, A., et al. (2017). Developmental expression of 4-repeat-tau induces neuronal aneuploidy in *Drosophila* tauopathy models. *Sci. Rep.* 7, 40764. <https://doi.org/10.1038/srep40764>.
- Mann, B.J., and Wadsworth, P. (2019). Kinesin-5 regulation and function in mitosis. *Trends Cell Biol.* 29, 66–79. <https://doi.org/10.1016/j.tcb.2018.08.004>.
- Mathys, H., Davila-Velderrain, J., Peng, Z., Gao, F., Mohammadi, S., Young, J.Z., Menon, M., He, L., Abdurrob, F., Jiang, X., et al. (2019). Single-cell transcriptomic analysis of Alzheimer's disease. *Nature* 570, 332–337. <https://doi.org/10.1038/s41586-019-1195-2>.
- Moore, A.M., Mahoney, E., Dumitrescu, L., De Jager, P.L., Koran, M.E.I., Petyuk, V.A., Robinson, R.A., Ruderfer, D.M., Cox, N.J., Schneider, J.A., et al. (2020). APOE epsilon4-specific associations of VEGF gene family expression with cognitive aging and Alzheimer's disease. *Neurobiol. Aging* 87, 18–25. <https://doi.org/10.1016/j.neurobiolaging.2019.10.021>.
- Mostafavi, S., Gaiteri, C., Sullivan, S.E., White, C.C., Tasaki, S., Xu, J., Taga, M., Klein, H.U., Patrick, E., Komashko, V., et al. (2018). A molecular network of the aging human brain provides insights into the pathology and cognitive decline of Alzheimer's disease. *Nat. Neurosci.* 21, 811–819. <https://doi.org/10.1038/s41593-018-0154-9>.
- Mullan, M., Crawford, F., Axelman, K., Houlden, H., Lilius, L., Winblad, B., and Lannfelt, L. (1992). A pathogenic mutation for probable Alzheimer's disease in the APP gene at the N-terminus of beta-amyloid. *Nat. Genet.* 1, 345–347. <https://doi.org/10.1038/ng0892-345>.
- Myers, K.A., and Baas, P.W. (2007). Kinesin-5 regulates the growth of the axon by acting as a brake on its microtubule array. *J. Cell Biol.* 178, 1081–1091. <https://doi.org/10.1083/jcb.200702074>.
- Nadar, V.C., Ketschek, A., Myers, K.A., Gallo, G., and Baas, P.W. (2008). Kinesin-5 is essential for growth-cone turning. *Curr. Biol.* 18, 1972–1977. <https://doi.org/10.1016/j.cub.2008.11.021>.
- Nesterov, E.E., Skoch, J., Hyman, B.T., Klunk, W.E., Bacskai, B.J., and Swager, T.M. (2005). In vivo optical imaging of amyloid aggregates in brain: design of fluorescent markers. *Angew. Chem. Int. Ed. Engl.* 44, 5452–5456. <https://doi.org/10.1002/anie.200500845>.
- O'Leary, T.P., Mantolino, H.M., Stover, K.R., and Brown, R.E. (2020). Age-related deterioration of motor function in male and female 5xFAD mice from 3 to 16 months of age. *Genes Brain Behav.* 19, e12538. <https://doi.org/10.1111/gbb.12538>.
- O'Leary, T.P., Robertson, A., Chipman, P.H., Rafuse, V.F., and Brown, R.E. (2018). Motor function deficits in the 12 month-old female 5xFAD mouse model of Alzheimer's disease. *Behav. Brain Res.* 337, 256–263. <https://doi.org/10.1016/j.bbr.2017.09.009>.
- Oakley, H., Cole, S.L., Logan, S., Maus, E., Shao, P., Craft, J., Guillozet-Bongaarts, A., Ohno, M., Disterhoft, J., Van Eldik, L., et al. (2006). Intraneuronal beta-amyloid aggregates, neurodegeneration, and neuron loss in transgenic mice with five familial Alzheimer's disease mutations: potential factors in amyloid plaque formation. *J. Neurosci.* 26, 10129–10140. <https://doi.org/10.1523/JNEUROSCI.1202-06.2006>.
- Penazzi, L., Tackenberg, C., Ghori, A., Golovyashkina, N., Niewidok, B., Selle, K., Ballatore, C., Smith, A.B., 3rd, Bakota, L., and Brandt, R. (2016). Abeta-mediated spine changes in the hippocampus are microtubule-dependent and can be reversed by a subnanomolar concentration of the microtubule-stabilizing agent epothilone D. *Neuropharmacology* 105, 84–95. <https://doi.org/10.1016/j.neuropharm.2016.01.002>.
- Penn, A.C., Zhang, C.L., Georges, F., Royer, L., Breillat, C., Hosi, E., Petersen, J.D., Humeau, Y., and Choquet, D. (2017). Hippocampal LTP and contextual learning require surface diffusion of AMPA receptors. *Nature* 549, 384–388. <https://doi.org/10.1038/nature23658>.
- Perez-Cruz, C., Nolte, M.W., van Gaalen, M.M., Rustay, N.R., Termost, A., Tanghe, A., Kirchhoff, F., and Ebert, U. (2011). Reduced spine density in specific regions of CA1 pyramidal neurons in two transgenic mouse models of Alzheimer's disease. *J. Neurosci.* 31, 3926–3934. <https://doi.org/10.1523/JNEUROSCI.6142-10.2011>.
- Potter, H., Chial, H.J., Caneus, J., Elos, M., Elder, N., Borysov, S., and Granic, A. (2019). Chromosome instability and mosaic aneuploidy in neurodegenerative and neurodevelopmental disorders. *Front. Genet.* 10, 1092. <https://doi.org/10.3389/fgene.2019.01092>.
- Reza-Zaldivar, E.E., Hernández-Sápiens, M.A., Minjarez, B., Gómez-Pinedo, U., Sánchez-González, V.J., Márquez-Aguirre, A.L., and Canales-Aguirre, A.A. (2020). Dendritic spine and synaptic plasticity in Alzheimer's disease: a focus on MicroRNA. *Front. Cell Dev. Biol.* 8, 255. <https://doi.org/10.3389/fcell.2020.00255>.
- Richard, B.C., Kurdakova, A., Baches, S., Bayer, T.A., Weggen, S., and Wirths, O. (2015). Gene dosage dependent Aggravation of the neurological phenotype in the 5xFAD mouse model of Alzheimer's disease. *J. Alzheimers Dis.* 45, 1223–1236. <https://doi.org/10.3233/JAD-143120>.
- Roman, F., Staubli, U., and Lynch, G. (1987). Evidence for synaptic potentiation in a cortical network during learning. *Brain Res.* 418, 221–226. [https://doi.org/10.1016/0006-8993\(87\)90089-8](https://doi.org/10.1016/0006-8993(87)90089-8).
- Roussarie, J.P., Yao, V., Rodriguez-Rodriguez, P., Oughtred, R., Rust, J., Plautz, Z., Kasturia, S., Albornoz, C., Wang, W., Schmidt, E.F., et al. (2020). Selective neuronal vulnerability in Alzheimer's disease: a network-based analysis. *Neuron* 107, 821–835.e12. <https://doi.org/10.1016/j.neuron.2020.06.010>.
- Scheff, S.W., Price, D.A., Schmitt, F.A., and Mufson, E.J. (2006). Hippocampal synaptic loss in early Alzheimer's disease and mild cognitive impairment. *Neurobiol. Aging* 27, 1372–1384. <https://doi.org/10.1016/j.neurobiolaging.2005.09.012>.
- Spires, T.L., Meyer-Luehmann, M., Stern, E.A., McLean, P.J., Skoch, J., Nguyen, P.T., Bacskai, B.J., and Hyman, B.T. (2005). Dendritic spine abnormalities in amyloid precursor protein transgenic mice demonstrated by gene transfer and intravital multiphoton microscopy. *J. Neurosci.* 25, 7278–7287. <https://doi.org/10.1523/JNEUROSCI.1879-05.2005>.
- Terry, R.D., Masliah, E., Salmon, D.P., Butters, N., DeTeresa, R., Hill, R., Hansen, L.A., and Katzman, R. (1991). Physical basis of cognitive alterations in Alzheimer's disease: synapse loss is the major correlate of cognitive impairment. *Ann. Neurol.* 30, 572–580. <https://doi.org/10.1002/ana.410300410>.
- Uhlen, M., Fagerberg, L., Hallström, B.M., Lindskog, C., Oksvold, P., Mardinoglu, A., Sivertsson, A., Kampf, C., Sjöstedt, E., Asplund, A., et al. (2015). Proteomics. Tissue-based map of the human proteome. *Science* 347, 1260419. <https://doi.org/10.1126/science.1260419>.
- Umeda, T., Ramser, E.M., Yamashita, M., Nakajima, K., Mori, H., Silverman, M.A., and Tomiyama, T. (2015). Intracellular amyloid beta oligomers impair organelle transport and induce dendritic spine loss in primary neurons. *Acta Neuropathol. Commun.* 3, 51. <https://doi.org/10.1186/s40478-015-0230-2>.
- Walker, C.K., and Herskowitz, J.H. (2020). Dendritic spines: mediators of cognitive resilience in aging and Alzheimer's disease. *Neuroscientist* 27, 487–505. <https://doi.org/10.1177/1073858420945964>.
- Wei, W., Nguyen, L.N., Kessels, H.W., Hagiwara, H., Sisodia, S., and Malinow, R. (2010). Amyloid beta from axons and dendrites reduces local spine number and plasticity. *Nat. Neurosci.* 13, 190–196. <https://doi.org/10.1038/nn.2476>.
- Wilson, R.S., Boyle, P.A., Yu, L., Barnes, L.L., Sytsma, J., Buchman, A.S., Bennett, D.A., and Schneider, J.A. (2015). Temporal course and pathologic basis of unawareness of memory loss in dementia. *Neurology* 85, 984–991. <https://doi.org/10.1212/WNL.0000000000001935>.
- Wu, H.Y., Hudry, E., Hashimoto, T., Kuchibhotla, K., Rozkalne, A., Fan, Z., Spires-Jones, T., Xie, H., Arbel-Ornath, M., Grosskreutz, C.L., et al. (2010). Amyloid beta induces the morphological neurodegenerative triad of spine loss, dendritic simplification, and neuritic dystrophies through calcineurin activation. *J. Neurosci.* 30, 2636–2649. <https://doi.org/10.1523/JNEUROSCI.4456-09.2010>.
- Xiao, N.A., Zhang, J., Zhou, M., Wei, Z., Wu, X.L., Dai, X.M., Zhu, Y.G., and Chen, X.C. (2015). Reduction of glucose metabolism in olfactory bulb is an earlier Alzheimer's disease-related biomarker in 5xFAD mice. *Chin. Med. J.* 128, 2220–2227. <https://doi.org/10.4103/0366-6999.162507>.
- Yoon, S.Y., Choi, J.E., Huh, J.W., Hwang, O., Lee, H.S., Hong, H.N., and Kim, D. (2005). Monastrol, a selective inhibitor of the mitotic kinesin Eg5, induces a distinctive growth profile of dendrites and axons in primary cortical neuron cultures. *Cell*

Motil. Cytoskelet. 60, 181–190. <https://doi.org/10.1002/cm.20057>.

Young-Pearse, T.L., Bai, J., Chang, R., Zheng, J.B., LoTurco, J.J., and Selkoe, D.J. (2007). A critical function for beta-amyloid precursor protein in neuronal migration revealed by in utero RNA interference. *J. Neurosci.* 27, 14459–14469. <https://doi.org/10.1523/JNEUROSCI.4701-07.2007>.

Zhang, B., Carroll, J., Trojanowski, J.Q., Yao, Y., Iba, M., Potuzak, J.S., Hogan, A.M.L., Xie, S.X., Ballatore, C., Smith, A.B., 3rd, et al. (2012). The microtubule-stabilizing agent, epothilone D, reduces axonal dysfunction, neurotoxicity, cognitive deficits, and Alzheimer-like pathology in an interventional study with aged tau transgenic mice. *J. Neurosci.* 32, 3601–3611. <https://doi.org/10.1523/JNEUROSCI.4922-11.2012>.

Zhang, B., Yao, Y., Cornec, A.S., Oukoloff, K., James, M.J., Koivula, P., Trojanowski, J.Q., Smith, A.B., 3rd, Lee, V.M.Y., Ballatore, C., and Brunden, K.R. (2018). A brain-penetrant triazolopyrimidine enhances microtubule-stability, reduces axonal dysfunction and decreases tau pathology in a mouse tauopathy model. *Mol. Neurodegener.* 13, 59. <https://doi.org/10.1186/s13024-018-0291-3>.

STAR★METHODS

KEY RESOURCES TABLE

REAGENT or RESOURCE	SOURCE	IDENTIFIER
Antibodies		
6E10	BioLegend	Cat#803001
Alexa Fluor® Plus 488-conjugated goat anti-mouse IgG secondary antibody	Invitrogen	Cat#A32723
Anti-GFP antibody	ThermoFisher	Cat#11122
Critical commercial assays		
RNeasy Mini Kit	Qiagen	Cat#74104
Experimental models: Organisms/strains		
Mouse: 5xFAD C57Bl/6 B6SJ-Tg(APP ^{Swe} FILon, PSEN1* ^{M146L} * ^{L286V})6799Vas/Mmjax	The Jackson Laboratory	RRID:MMRRC_034840-JAX
Mouse: Pim1-Kin5OE (referred to herein as Kif11OE)	Dr. Monica Justice (Castillo et al., 2007)	Tg(Pim1-Eg5)1Jus
Mouse: C57BL/6J	The Jackson Laboratory	RRID:IMSR_JAX:000664
Rat: Sprague Dawley Charles River	Charles River	Cat#RGD_734476
Oligonucleotides		
KIF11 Primer Probe	Applied Biosystems	Cat#Mm01204225_m1 Cat#4448489
APP Primer Probe	Applied Biosystems	Cat#Hs0016908_m1 Cat#4331182
GAPDH Primer Probe	Applied Biosystems	Cat#Mm99999915_g1 Cat#4331182
Tg(Pim1-Eg5)1Jusm (KIF11OE) forward primer 5'-TGACTTCCGATGAAGAAAGC-3'	Integrated DNA Technologies (IDT) (Castillo et al., 2007)	N/A
Tg(Pim1-Eg5)1Jus (KIF11OE) reverse primer 5'-GATACACGGGTACCCGGGCG-3'	Integrated DNA Technologies (IDT) (Castillo et al., 2007)	N/A
APP forward primer 5'-TGGGTTCAAACAAGGTGCAA-3'	Integrated DNA Technologies (IDT)	N/A
APP reverse primer 5'-GATGACGATCACTGTCGCTATGAC-3'	Integrated DNA Technologies (IDT)	N/A
Recombinant DNA		
Wild-type Kif11 expression plasmid	Dr. Peter Baas (Myers and Baas, 2007)	N/A
APP ^{Swe/Ind} expression plasmid	Addgene (http://www.addgene.org/30145)	Cat#30145; RRID:Addgene_30145
pEGFPN1	Clontech	Cat#6085-1
Software and algorithms		
Slidebook 5.0–6.0	Intelligent Imaging Innovations	https://www.intelligent-imaging.com/slidebook
R statistical software	https://www.r-project.org	N/A
Prism 9	GraphPad	https://www.graphpad.com/scientific-software/prism/
Other		
NIAD-4 (amyloid stain)	Cayman Chemical	Cat#18520
Hoechst 33342 (Nuclear stain)	Thermo Scientific	Cat#62249
Extracta DNA Prep for PCR	Quantabio	Cat#95091
Neurobasal Plus B27	Invitrogen	Cat#A3582901
Glutamax	Invitrogen	Cat#35050061
TRlzo™ Reagent	Invitrogen	Cat#15596018

RESOURCE AVAILABILITY

Lead contact

Further information and requests should be directed to and fulfilled by the lead contact, Huntington Potter (huntington.potter@cuanschutz.edu).

Resource availability

- This study did not generate new unique reagents.
- Kif11OE mice on C57BL/6 background will be made available from the [lead contact](#) upon request.
- Any available biological samples from 5xFAD-Kif11OE mice are available from the [lead contact](#) upon request.

Data and code availability

- This study does not report any original code.
- The data reported in this paper as well as any additional information required to reanalyze the data reported is available from the [lead contact](#) upon request.

EXPERIMENTAL MODEL AND SUBJECT DETAILS

Animals

Male and female 5xFAD (Oakley et al., 2006) or Kif11OE (Tg[Pim1-Eg5]Jus mice) (Castillo et al., 2007), referred to herein as Kif11OE mice, were used for breeding and for generation of the 5xFAD-Kif11OE transgenic mouse strain. Fully congenic male and female C57Bl/6J mice hemizygous for the 5xFAD transgenes that contain three mutations in human APP (Swedish: K670N, M671L, Florida: I716V, and London: V717I) and two mutations in human PSEN1 (M146L and L286V) (Oakley et al., 2006) were obtained from Jackson Labs (JAX MMRRC Stock No: 34848-JAX). These mice were used to establish an in-house breeding colony in which 5xFAD mice were bred to fully congenic WT C57Bl/6J mice obtained from Jackson labs (Jax Stock Number: 000664). Establishment of the 5xFAD breeding colony took place in-house and utilized both male and female mice bred with respective WT C57Bl/6J mice obtained from Jackson Laboratory. To establish the Kif11OE colony, we obtained cryo-preserved semen from fully congenic FVB/NJ male mice harboring the pPim1E μ -Eg5 transgene (Kif115OE) from the laboratory of Dr. Monica Justice at The Hospital for Sick Children, Peter Gilganis Centre for Research and Learning, Toronto, Ontario, Canada. This mouse model utilizes the pPim1E μ -Eg5 transgene where the lymphoid specific E μ enhancer in tandem with the Pim1 promoter drive the expression of mouse Kif11. The transgene also contains the MuLV long terminal repeat to further amplify expression. Rederivation of the transgenic mouse line was carried out through *in vitro* fertilization (IVF) by the University of Colorado Anschutz Medical Campus Gates Bioengineering Core. Briefly, mouse oocytes were generated using a fully congenic WT C57Bl/6J female mouse, creating mixed background (C57Bl/6J-FVB/NJ) Kif11OE progeny. Kif11OE mice produced through the rederivation processes were bred strictly with non-related fully congenic C57Bl/6J WT mice to backcross the mice to a predominant C57Bl/6J background. Breeding took place in-house and utilized both male and female mice from each group. We continued to backcross the Kif11OE mice with fully congenic C57Bl/6J mice throughout the entirety of this study. To develop a 5xFAD Alzheimer's mouse model that overexpresses mouse Kif11 (5xFAD-Kif11OE), we used unrelated male and female mice that carried either the 5xFAD transgenes or the Kif11OE transgene for breeding. Kif11OE mice from the F4-F9 C57Bl/6J backcross generation were then bred with fully congenic C57Bl/6J 5xFAD mice to create a mouse line that was predominantly on a C57Bl/6J background (93%–99% C57Bl/6J). Only mice derived from the 5xFAD x Kif11OE cross were used in experiments. Both male and female 6- to 8-month-old mice were used for electrophysiology experiments and for behavioral tests in the RAWM. The mice utilized for study were subject to either behavioral tests or LTP recordings. No animals were used for both. The brains of mice that underwent behavioral tests were used for immuno-histochemistry experiments for AD pathology or for qPCR analyses of gene expression. All mouse experiments and husbandry were approved by and conducted in accordance with the Institutional Animal Care and Use Committee (IACUC) guidelines and with approval from the University of Colorado Anschutz Medical Campus.

Primary neuron cultures

Wild-type non-transgenic postnatal day 0–2 male and female Sprague-Dawley rats used for primary cultures were obtained from timed pregnant female Sprague-Dawley rats supplied by Charles Rivers Labs. All animals used in this study were fed standard chow and kept on a regular 12:12 light cycle. Primary neuronal cultures were incubated and maintained at 33°C in 5% CO₂. All experiments were approved by and conducted in accordance with the IACUC guidelines and with approval from the University of Colorado Anschutz Medical Campus.

Human

Data for the analysis of human subjects was acquired from the Religious Orders Study and the Rush Memory and Aging Project (ROS/MAP) under a master data users agreement to the University of Colorado Anschutz Medical Campus with access to the data used in this study granted to Drs. Esteban M. Lucero and Huntington Potter. Written informed consent was previously obtained for the generation of the data used in this study in accordance with Institutional Review Board (IRB) approved protocols. ROSMAP data are available online at the Rush Alzheimer's Disease Center Resource Sharing Hub and the Accelerating Medicines Partnership-Alzheimer's Disease (AMP-AD) Knowledge Portal (syn3219045).

METHOD DETAILS

Genotyping of transgenic mouse lines

To obtain tissue samples for genotyping, small ear clips were taken from 21- to 28-week-old mice anesthetized with 4% isoflurane. At that time, the mice were also given a subcutaneous radio frequency radio identification (RFID) tag (Trovan, Ltd, cat: 040104) and weaned from the mother. DNA was extracted from the ear tissue using Extracta DNA Prep (Quantabio) according to manufacturer guidelines. Briefly, the tissue was incubated for 30 min at 95°C in 300 μ L extraction reagent, cooled to room temperature, and 300 μ L stabilization buffer was then added to the sample. PCR Genotyping of Kif11OE mice for the *pPim1E μ -Eg5* transgene was carried out using the protocol established by [Castillo et al.\(2007\)](#). Primers specific to Kif11 (5'-TGACTTCCGATGAAGAAAGC-3') and the MuLV LTR of the transgene construct (5'-GATACACGGGTACCCGGGCG-3') were used with an annealing temperature of 58°C and 20 cycles of PCR. The resulting PCR products were then run on a 1% agarose gel that revealed binary results, where samples that yielded a single \sim 1,000 bp band were considered to be positive for the *pPim1E μ -Eg5* transgene, and samples that yielded no band were considered non-transgenic (WT). 5xFAD mice were genotyped according to guidelines established by Jackson Labs (<https://www.jax.org/Protocol?stockNumber=008730&protocolID=34650>). Briefly, a primer probe specific to the APP_{Swe} mutation (TmolMR0076-Fluorophore-1 5'-CATTGGACTCATGGTGGGGGGGGGTG-3') was paired with primers specific to the APP_{Swe} transgene in the 5xFAD mouse (5'-TGGGTTCAAACAAAGGTGCAA-3', 5'-GATGACGATCACTGTCGCTATGAC-3') and subjected to 40 cycles of RT-PCR with an annealing temperature of 60°C. Samples that showed amplification of the PCR product through real-time fluorescence after 20 cycles were considered positive for the 5xFAD transgene, and samples that did not show any amplification during the 40 cycles were considered to not contain the 5xFAD transgene. PCR genotyping for each mouse strain used PerfeCTa® MultiPlex qPCR SuperMix, Low ROX™ (Quantabio, cat: 95063) at a 1X concentration.

Gene expression analyses

Both *APP* and *Kif11* expression were analyzed using qRT-PCR. Whole brains were extracted from mice anesthetized with 100 μ L pentobarbital. Once anesthetized, the mice were sacrificed using cervical dislocation and decapitation, and the brain was quickly removed and quartered. The quartered pieces of each brain were placed into individual RNase-free 2 mL microfuge tubes and flash frozen with liquid nitrogen. Brain tissue samples were homogenized using ultrasonication in 1 mL of 35°C Trizol (Invitrogen cat: 15596018). The samples were incubated for 5 min at room temperature and vortexed for 10 sec intermittently during the incubation. To extract the RNA, 200 μ L chloroform was added to each sample, followed by vortexing for 15 sec, incubation for 1 min at room temperature, vortexing for 15 sec, and centrifugation at 13,000 \times g for 10 min. The supernatant was then collected for the isolation and purification of the RNA using the RNeasy Mini Kit (QIAGEN, cat: 74104) according to manufacturer instructions. After the RNA was eluted, cDNA was synthesized using the iScript™ cDNA synthesis Kit (Bio-Rad). Expression levels of *Kif11* and *APP* were then measured by multiplex qRT-PCR using mouse *Kif11* and human *APP* primer probes (Applied Biosystems, Mm01204225_m1, Cat#4448489 and Hs0016908_m1 Cat#4331182, respectively) in

combination with mouse *GAPDH* primer probes (Applied Biosystems Cat#4331182/AssayID-Mm99999915_g1) for normalization. Expression levels were calculated as the log₂-fold change of the $\Delta\Delta C_t$.

Radial arm water maze (RAWM)

We measured working memory in our mouse models using the performance of each mouse in a six-arm RAWM (Alamed et al., 2006). We used modular plastic inserts placed inside a water tank to create six radially distributed swim arms emanating from a central circular swim area. The tank was placed on a table so that the top of the tank was approximately 6.5 feet from the ground. This allowed the test to take place without visual cues from the surrounding room environment and eliminated influence of the performance of the mouse that might be caused by activities of the people administering the test. Visual cues to facilitate spatial awareness of the mouse were not added to the maze. The tank was filled with water the night prior to testing to allow the water to reach room temperature, and the water was dyed white with non-toxic water-soluble paint on the morning of testing. An escape platform made of translucent plexiglass was placed in one of the six arms and remained in that same arm throughout the testing. Prior to the beginning of testing on day one of the two-day-long test, the mouse was introduced to the maze by placing it on the submerged platform and allowing it to remain there for 60 sec. Afterwards, the mouse was placed in its holding cage until the beginning of the test. Mice were tested in groups of 2–4 mice per block of testing, with each mouse per group undergoing the test sequentially, which allowed each mouse to rest between trials during that block of testing. After the mice from each group had completed each block of trials, each mouse was then placed in one of the five arms that did not contain the escape platform and was given 60 sec to complete the maze. If the mouse failed to complete the maze in 60 sec, the mouse was guided to the platform with a wooden guiding board and allowed to place itself on the platform where it remained for 60 sec. Each mouse underwent two days of testing with 15 trials per day. The performance of each mouse was measured using both the time (latency) and the number of errors the mouse made during testing. Errors were considered when the mouse fully entered (i.e., entire body) an arm that did not contain the escape platform or when the mouse entered the correct arm with the escape platform but did not swim to or locate the escape platform. Measurements of performance relative to the average performance of the WT group were calculated as the percent difference of each mouse at each block compared to the average performance of the WT group at each block. Statistical analyses for RAWM performance used GraphPad Prism software version 9.0.2 (<https://www.graphpad.com/scientific-software/prism/>).

Electrophysiology

Electrophysiology recordings for LTP measurements were carried out on transverse 400 μm -thick hippocampal slices (Freund et al., 2016) from mice that had not undergone behavioral testing in the RAWM. All of the mice used for electrophysiology experiments were progeny of 5xFAD x Kif11OE breeding. Mice were anesthetized with isoflurane, decapitated, and the brain was removed. To cool the interior of the brain, the entire brain was placed in ice-cold cutting solution containing 220 mM sucrose, 25 mM D-Glucose, 2 mM KCl, 12 mM MgCl₂, 0.2 mM CaCl₂, 1.25 mM NaH₂PO₄, and 26 mM NaHCO₃ for 60 sec. Afterwards, the hippocampi were dissected from the brain and sliced transversely with a McIlwain tissue slicer. Once the slices were made, they were placed in a recovery chamber containing artificial cerebral spinal fluid (aCSF) (124 mM NaCl, 11 mM D-glucose, 3.5 mM KCl, 1.3 mM MgCl₂, 2.5 mM CaCl₂, and 25.9 mM NaHCO₃) for at least 1 h. Individual hippocampal slices were then transferred to a recording chamber superfused at a bulk rate of 2–3 mL/min with 30°C aCSF. To measure fEPSP responses, we placed stimulus and recording electrodes in the collateral axon pathway of the CA1 dendritic field. Measurements of the fEPSP response were an average of three responses to stimuli delivered 20 sec apart. Prior to baseline recordings, we generated an input-output curve by increasing the stimulus voltage and recording the synaptic response until either a maximum response was reached, or until a population spike was observed in the fEPSP response. Stimulus intensity was set at 40–50% of the maximum stimulus intensity. Once proper stimulus intensity was determined, we took baseline recordings of the fEPSP response at a stimulus intensity specific to each slice. Baseline recordings were measured for 20 min, after which we administered HFS. HFS consisted of two trains of 100 Hz stimulation for 1 sec, with an intertrain interval of 5 min. Measurements of the fEPSP response to stimulus were monitored for 60 min after the first HFS was delivered. Statistical analyses for the measurement of LTP as a percent of baseline recording was calculated using GraphPad Prism version 9.0.2 (<https://www.graphpad.com/scientific-software/prism/>).

Neuronal cultures

Hippocampal neuronal cultures were prepared from postnatal day 0–2 male and female Sprague-Dawley rats, plated at medium density (300–450 cells/mm²) on glass coverslips and maintained at 33°C in ~5% CO₂ in Neurobasal plus B27 (Invitrogen) and GlutaMAX (Invitrogen) medium until transfection on day-*in-vitro* (DIV) 11–12 using Lipofectamine 2000 (Invitrogen) as described with plasmids encoding green fluorescent protein (GFP) (pEGFPN1; Clontech), mouse *Kif11* (Myers and Baas, 2007), or the human APP_{Swe/Ind} mutant (Young-Pearse et al., 2007). On DIV 14–15 (three days post-transfection), neurons were fixed in 4% paraformaldehyde, and the coverslips were mounted on slides with Pro-Long Gold (Invitrogen). Images of dendrites in GFP-transfected neurons were acquired on an Axiovert 200M microscope (Zeiss) with a 63X objective (1.4NA, plan-Apo), a 1.5X magnifier, and a CoolSNAP2 (Photometrics) CCD camera. Focal plane Z-stacks (0.5 μm sections) were acquired, deconvolved to correct for out-of-focus light, and 2D maximum intensity projections generated (Slidebook 5.0–6.0, Intelligent Imaging Innovations). Spine numbers were quantified from projection images using the ruler tool in Slidebook 5.0–6.0 software with manual counting and were expressed as the number of spines/10 μm of dendrite using measurements obtained for multiple lengths of dendrites (N = the number of lengths of dendrite) taken from multiple images across three independent neuronal cultures for each experimental treatment condition. Statistical analyses for dendritic spine density used GraphPad Prism version 9.0.2 (<https://www.graphpad.com/scientific-software/prism/>).

Mouse brain collection and amyloid staining

To determine amyloid plaque burden in our mouse models, we used 20 μm-thick sagittal cryo-sectioned mouse brains. Prior to cryosectioning, the mice were anesthetized with 100 μL of pentobarbital. Once fully anesthetized, transcardial perfusion was performed with 0.9% NaCl in H₂O. A Leica Biosystems Perfusion Two™ automated pressure perfusion system (cat: 39471005) was used to circulate the saline solution. Mice were perfused until the liver of the mouse showed evidence of being clear of blood or for 5 min after the start of perfusion. After perfusion, the brain was removed rapidly, and the hemispheres were separated. The two hemispheres were then placed in 10 mL of 4% paraformaldehyde in PBS for 72 h. The brains were then transferred into a 20% sucrose solution for 24 h and placed in a 30% sucrose solution and stored at 4°C until slicing. At 12–24 h before slicing, the brains were removed from the sucrose solution and placed in a 50 mL conical tube and stored at –80°C. On the day of cryosectioning, one hemisphere of the brain was placed inside the cryostat for 1 h to allow for acclimation to the –20°C environment. The brain hemisphere was then embedded in chilled Tissue Tek® O.C.T.™ compound and incubated for 30 min inside the cryostat. Sagittal sections of the brain were obtained by slicing the brain at 20 μm laterally from the midline. Each slice was then placed onto a Fisherbrand® Superfrost™ Plus Microscope Slide (cat: 12-550-15) and placed into a slide box on dry ice and stored at –80°C until staining.

For amyloid staining, tissue sections were permeabilized with 0.1% Triton X-100 in DPBS for 15 min and then blocked with 3% bovine serum albumin (BSA) in DPBS for 90 min at room temperature. Tissue sections were incubated with mouse anti-Aβ primary antibody (6E10, BioLegend #803014, 1:250) in 3% BSA in DPBS overnight at 4°C, followed by incubation with Alexa Fluor® Plus 488-conjugated goat anti-mouse IgG secondary antibody (Invitrogen #A32723, 1:500) in 3% BSA in DPBS for 45 min at room temperature. Tissue sections were then stained with the amyloid-binding dye NIAD-4 (Cayman Chemical #18520) at 10 μM in DPBS for 10 min at room temperature, and the nuclei were stained using Hoechst 33342 (Thermo Scientific #62249) at 1 μg/mL in DPBS for 10 min at room temperature. Slides were imaged on an Olympus IX83 inverted fluorescence microscope at 10X magnification and then analyzed using Cell Sens v1.12 software (Olympus). Data from 2–5 tissue sections were averaged for each mouse.

ROS/MAP study analyses

The Religious Orders Study and the Rush Memory and Aging Project (ROS/MAP) (Bennett et al., 2018) began collecting data in 1994 and 1997, respectively. Together, the two longitudinal studies have followed Catholic clergy from throughout the United States ROS and individuals from the greater Chicago area (MAP) who were without known dementia at the time of enrollment). Both studies were approved by an Institutional Review Board of Rush University Medical Center. All participants signed an informed consent, an Anatomic Gift Act, and a repository consent that allowed their data and biospecimens to be shared. Collectively, these studies have generated a wealth of data including longitudinal measurements of cognitive function throughout the course of aging as well as, in some cases, during the onset and progression of AD. Participants in both studies also underwent annual clinical evaluations. During the clinical evaluations, five domains of cognition were evaluated (i.e., episodic memory, semantic memory, working memory,

perceptual orientation, and perceptual speed) using 17 different tests from established protocols (Bennett et al., 2018; Wilson et al., 2015). The average z-scores produced by these quantitative evaluations were used to compute global cognition scores that were previously measured and published (Bennett et al., 2012a, 2012b) and made available for correlative analyses. In addition to longitudinal cognitive measurements, the participants also consented to donate their organs at the time of their death, thus allowing for post-mortem analyses of *KIF11* mRNA expression levels and pathological measures in brain. The processing of the genomic sequencing data (Illumina HiSeq platform) from frozen sections of a third of the DLPFC (Lim et al., 2014; Mostafavi et al., 2018) were made available for our study. The remaining DLPFC, and the PCC and the head of the CN were processed similarly. Data are available on the AMP-AD Knowledge Portal (syn3219045) as well as the Rush Alzheimer's Disease Center Resource Sharing Hub (<https://www.radc.rush.edu>). Data processing followed a published protocol (Logsdon et al., 2019) including alignment to GRCh38 with STAR (v2.5.2b) and gene counting with feature Counts from subread (v2.0.0). RNAseq quality control (QC) included the removal of samples for low RIN (< 4), high postmortem interval (> 24 h), and missing GC content.

QUANTIFICATION AND STATISTICAL ANALYSIS

Analyses of data from human subject in the ROS/MAP study were completed in R (Version 3.5.1, <https://www.r-project.org>). Cross-sectional analyses with cognitive performance at the final visit were performed using linear regression, and longitudinal analyses of cognitive trajectories prior to death were performed using linear mixed-effects models with the intercept and interval (time from last visit modeled in years) included as fixed and random effects in the model. All models were covaried for age at death, sex, post-mortem interval, and the interval between the final cognitive assessment and death. Quantification and statistical analyses for all other experiments used GraphPad Prism version 9.0.2 (<https://www.graphpad.com/scientific-software/prism/>) to perform ordinary one-way ANOVA and post-hoc Holm-Šidák's multiple comparisons tests, with statistical significance measured at $p \leq 0.05$. Data are presented as the mean with error bars representing \pm of the standard error of the mean. Specific details of the analysis of data presented in this study, including sample size and for the statistical tests used for each analysis are outlined in each figure legend corresponding to those data.